www.advintellsyst.com

# Roads to Smart Artificial Microswimmers

Alan C. H. Tsang, Ebru Demir, Yang Ding,\* and On Shun Pak\*

Artificial microswimmers offer exciting opportunities for biomedical applications. The goal of these synthetics is to swim like natural micro-organisms through biological environments and perform complex tasks such as drug delivery and microsurgery. Extensive efforts in the past several decades have focused on generating propulsion at the microscopic scale, which has engendered a variety of artificial microswimmers based on different physical and physicochemical mechanisms. Yet, these major advancements represent only the initial steps toward successful biomedical applications of microswimmers in realistic scenarios. A next step is to design "smart" microswimmers that can adapt their locomotion behaviors in response to environmental factors. Herein, recent progress in the development of microswimmers with intelligent behaviors is surveyed in three major areas: 1) adaptive locomotion across different media, 2) tactic behaviors in response to environment stimuli, and 3) multifunctional swimmers that can perform complex tasks. The emerging technologies and novel approaches used in developing these "smart" microswimmers, which enable them to display behaviors similar to biological cells, are discussed.

#### 1. Introduction

#### 1.1. Swimming under the Microscope

In his 1959 talk entitled "There's Plenty of Room at the Bottom," Richard Feynman fantasized about swallowing a "microsurgeon" that can roam inside his blood vessels and perform microsurgery. [1] Such a microrobot would need to overcome stringent

Dr. A. C. H. Tsang, Dr. E. Demir, Prof. O. S. Pak Department of Mechanical Engineering Santa Clara University Santa Clara, CA 95053, USA E-mail: opak@scu.edu Dr. A. C. H. Tsang Department of Bioengineering Stanford University

Dr. E. Demir, Prof. Y. Ding Mechanics Division Beijing Computational Science Research Center Haidian, Beijing, China E-mail: dingyang@csrc.ac.cn

The ORCID identification number(s) for the author(s) of this article can be found under https://doi.org/10.1002/aisy.201900137.

© 2020 The Authors. Published by WILEY-VCH Verlag GmbH & Co. KGaA, Weinheim. This is an open access article under the terms of the Creative Commons Attribution License, which permits use, distribution and reproduction in any medium, provided the original work is properly cited.

DOI: 10.1002/aisy.201900137

constraints imposed by physics within the microscopic world to swim. Inertial effects, which govern macroscopic locomotion, become subdominant to viscous forces at small scales. The Revnolds number (Re), which characterizes the inertial to viscous forces, typically ranges from 10<sup>-6</sup> for flagellated bacteria to  $10^{-2}$  for spermatozoa. These micro-organisms have evolved different mechanisms to move through fluids to conduct a range of biological processes, including reproduction, foraging, and escaping from predators. [2-4] Many of these swimming micro-organisms use one or more appendages, called flagella and cilia (short flagella), for propulsion (Figure 1a-c). Some eukaryotic cells (e.g., sea-urchin spermatozoa Figure 1a) propel by propagating deformation waves along their flexible flagella, due to the action of molecular motors (dyneins) between adjacent microtubules within the flagellum.<sup>[3]</sup> In contrast, flagella of prokaryotic cells

(e.g., bacteria *Escherichia coli* and *Vibrio alginolyticus*) have structures and actuation mechanisms different from that of eukaryotic flagella. The prokaryotic flagellum is a rigid helical filament with a hook connecting to a rotary motor embedded in the cell wall. [11] Prokaryotic cells generate propulsion by rotating their passive helical flagella with the rotary motor (Figure 1a). Some microorganisms such as *Paramecium* and *Volvox* (Figure 1c) swim by beating arrays of cilia covering their surfaces. The cilia beat in a coordinated manner to generate metachronal waves for propulsion. [12] Extensive hydrodynamic analyses of these biological microswimmers have improved our general understanding of low-Reynolds-number locomotion. [13–16]

The motility and sensing capabilities of swimming microorganisms can be harnessed for biomedical applications. For instance, drug-loaded micro-organisms are capable of performing targeted drug delivery using their tactic responses to navigate toward infectious cells.  $^{[17-20]}$  Compared with artificial swimmers as delivery systems, these biological cells have the advantages of being autonomous in vivo, multiplying selectively in targeted sites, inhibiting growth of disease sites, and operating effectively under deep tissue. However, the biocompatibility of therapeutic solutions based on the use of biological cells has not been completely validated yet. Biovariability among different cells, inflammation caused by continuous cell reproduction and cell mutation over time can impose additional threat to their performance and raise safety concerns. [21] Complementary to the use of biological cells, recent developments in synthetic biology provides techniques to engineer biological cells with desirable properties. Biological cells can be genetically modified to

Stanford, CA 94305, USA

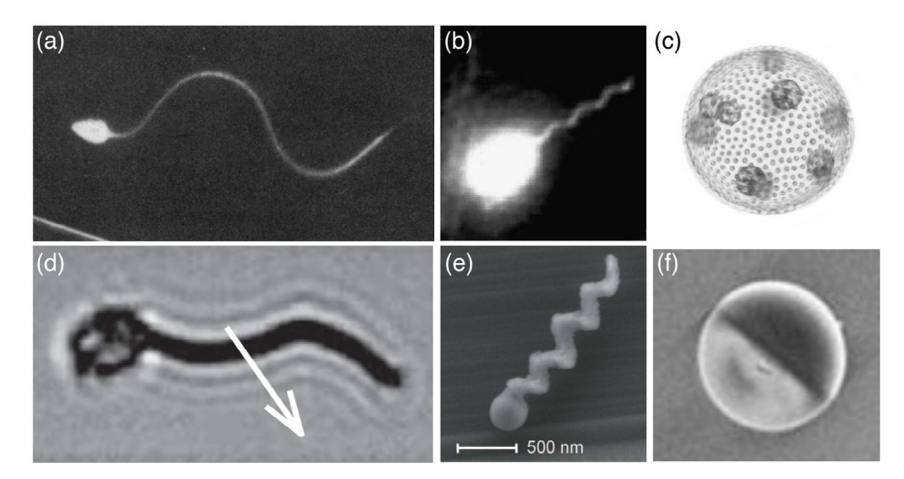


Figure 1. Biological (top row) and artificial (bottom row) swimmers at small scales. a) A sea-urchin spermatozoon with planar flagellar beating. Reproduced with permission. [5] Copyright 1985, Biophysical Society. b) A bacterium (*V. alginolyticus*) propelling with a rotating helical flagellum. Reproduced with permission. [6] Copyright 2001, Federation of European Microbiological Societies. c) Propulsion of a *Volvox* with coordinated beating of cilia covering its surface. Reproduced under a Creative Commons Attribution License (CC BY 4.0). [7] Copyright 2016, Cambridge University Press. d) A flexible propeller exploiting elastohydrodynamic interaction between its magnetic filament and its surrounding fluid for propulsion. Reproduced with permission. [8] Copyright 2005, Nature Publishing Group. e) A magnetic swimmer propelling by rotating its rigid, artificial helical flagellum under magnetic actuation. Reproduced with permission. [9] Copyright 2009, American Chemical Society. f) A Janus (Pt—SiO<sub>2</sub>) catalytic motor propelling by generating the local gradients of chemical concentration due to asymmetric surface chemistry. Reproduced under a Creative Commons Attribution License (CC BY 4.0). [10] Copyright 2016, Springer Nature.

introduce additional capabilities that are of interest for biomedical applications, such as environmental sensing, production and delivery of therapeutic agents in vivo, and performing synchronized cycles of cell breakdown and drug delivery. [22–24] An alternative approach is to design artificial micromachines and equip them with capabilities similar to biological cells. Compared with the millennia of natural evolution, advances in artificial microswimmers in the past decades represent initial success and call for further developments. As a third viable choice for biomedical applications, the biohybrid approach aims at leveraging the advantages of both biological and artificial systems. The pros and cons of these approaches depend on specific applications and environmental constraints. We refer the reader to reviews on synthetic biological microswimmers and bio-hybrid microswimmers<sup>[25–30]</sup> for further information about their recent developments and applications. In this Report, we focus on advances in artificial microswimmers and discuss recent progress toward making them "smart."

Earlier efforts in developing artificial microswimmers have focused on the capability to generate self-propulsion at the microscopic scale, which have engendered a variety of propulsion mechanisms (Figure 1d-f). While some artificial microswimmers are biomimetic or bioinspired (e.g., flexible and helical propellers that resemble spermatozoa and bacterial flagella, Figure 1d,e), other swimmers exploit physical and physicochemical mechanisms (e.g., catalytic Janus motors) that do not stem from the biological world to achieve micropropulsion (Figure 1f). The flexible propellers consist of flexible structures made of magnetic particles linked by DNA<sup>[8]</sup> (Figure 1d) or nanowires, which exploit fluid–structure interaction with the surrounding fluid to induce deformations that lead to propulsion. Magnetic helical propellers are helical microstructures which undergo rotation under the action of an external magnetic

field<sup>[9,37]</sup> (Figure 1e), mimicking the propulsion of helical bacterial flagella. Self-phoretic particles contribute another important class of microswimmers, which propel by generating local gradients of chemical concentration (self-diffusiophoresis) or electric potential (self-electrophoresis) via asymmetric surface reactions. For instance, Janus (Pt–SiO<sub>2</sub>) catalytic motors self-propel by generating local gradients of solute concentration due to its asymmetric chemical compositions (Figure 1f). We refer the readers to comprehensive reviews of various propulsion mechanisms for further details.<sup>[13,15,38,39]</sup>

## 1.2. "Smart" Artificial Microswimmers

Achieving the capability to swim in the absence of inertia like micro-organisms constitutes a major advancement on the development of artificial microswimmers over the past decades. Yet, this capability represents only the first step toward successful biomedical or environmental applications of microswimmers in practical scenarios. In their in vivo applications, biomedical microswimmers will often encounter complex biological environments with varying properties. Despite significant progress over the past decades, existing microswimmers are typically designed to have fixed locomotory gaits for a particular type of medium or environmental condition. Their capability of traversing heterogeneous, dynamically changing environments in a robust and autonomous manner remains an outstanding challenge. The conventional propulsion strategy is even harder to apply when the microswimmers need to move through environments whose properties (e.g., rheology of biological fluids, spatial landscapes, or heterogeneity of the environment) are poorly characterized or even unknown. The presence of unpredictable environmental factors adds further complexities to these applications. In these scenarios, external interventions such as

www.advintellsvst.com



adjusting swimmer's dynamics with actuation fields manually could become ineffective or impractical depending on the time and length scales involved. This points to a need to develop artificial microswimmers with adaptive locomotion like biological cells. In addition to robust locomotion strategies, the capability to respond to various environmental cues (e.g., biological and chemical signals) will aid the autonomous navigation of microswimmers to desired locations, in applications such as targeted drug delivery or environmental remediation. Finally, additional functionalities, such as more advanced and stable manipulations of micro-objects and the ability to perform multiswimmer operations, will arm these microswimmers to perform complex tasks in an autonomous manner. To achieve these goals, a next step is to design "smart" microswimmers, which we broadly define as microswimmers that can adapt their locomotion behaviors in response to environmental factors, including changes in their surrounding media or neighboring swimmers. In this perspective, we discuss recent progress in the development of these "smart" microswimmers in three major areas (Figure 2): 1) adaptive locomotion across different media, 2) tactic swimmers in response to external stimuli, and 3) multifunctional swimmers for performing complex tasks. We also discuss the emerging technologies and novel approaches used to instill the aforementioned intelligent behaviors into artificial microswimmers.

## 2. Adaptive Locomotion of Artificial Swimmers

Swimming at the microscopic scale by itself is a challenging task due to stringent physical constraints imposed by the absence of inertia. As described in Section 1, complexities present in diverse biological environments impose additional challenges to successful biomedical applications of microswimmers. These microswimmers need to traverse vastly different biological environments, including blood–brain, gastric mucosal barriers, and tumor microenvironments. At 1-43 However, locomotory gaits that are

optimal in one medium may become ineffective in a different medium; hence, locomotion performance of synthetic microswimmers with fixed locomotory gaits may not be robust to environmental changes. In contrast, natural organisms show robust locomotion performance across varying environments by adapting their locomotory gaits to the surroundings. [44–46] Without adaptability like their biological counterparts, it remains formidable for synthetic microswimmers to operate in complex biological media with unpredictable environmental factors. Recent developments have used a variety of novel materials and techniques to realize adaptive microswimmers, [47] which we discuss in the following sections.

## 2.1. Exploiting Soft Active Materials

The elastohydrodynamic interaction between flexible bodies and the surrounding fluid has been exploited by both biological and artificial microswimmers for propulsion. Some micro-organisms have distributed molecular motors along their flexible flagella, whose coordinated activity leads to flagellar beating and effective locomotion. [3,13] In contrast, artificial flexible swimmers, consisting of magnetic particles linked by DNA, [8] DNA assemblies, [48] nanowires, [35,36] typically deform only passively, [35,36,48] or have a small number of passive degrees of freedom (DOFs).[8] More recent developments on soft active materials, which deform in response to external stimuli such as light, [49-53] heat, [54-59] and magnetic field, [60,61] offer a class of shape-programmable materials to achieve mechanical functionalities beyond those of traditional soft materials. We highlight recent applications of these novel materials in the following paragraphs in realizing adaptive locomotion at small scales.

#### 2.1.1. Light-Driven Soft Microswimmers

Liquid-crystal elastomers (LCEs) are soft active materials that exhibit reversible shape changes in response to heat or light.<sup>[49]</sup>

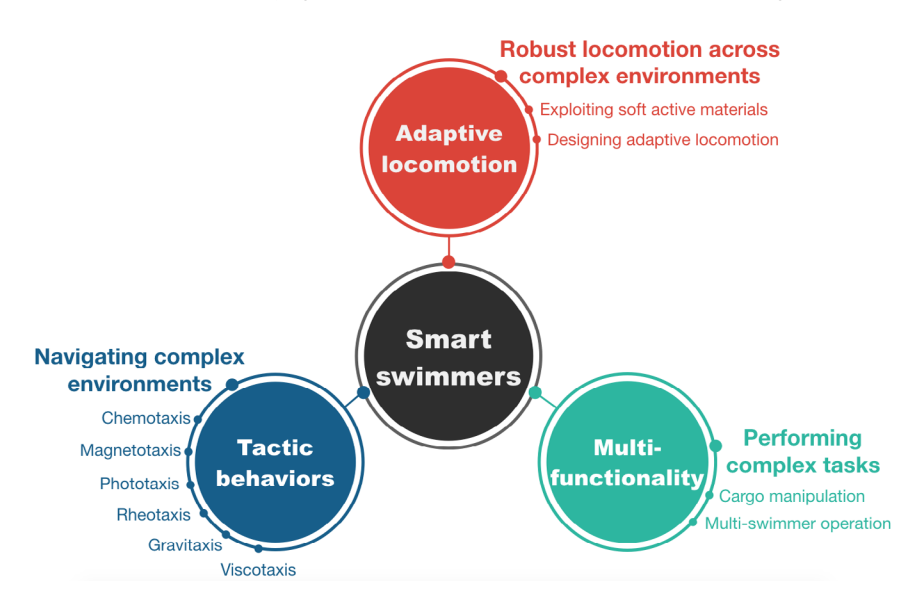


Figure 2. Overview of roads to smart artificial microswimmers. Herein, we report recent progress in the development of smart microswimmers in three major areas: adaptive locomotion across different media (Section 2), tactic behaviors in response to external stimuli (Section 3), and multifunctionality for performing complex tasks (Section 4).

www.advintellsvst.com

local light field from an external optical system (Figure 3a–d). The high spatial selectivity permits a large number of degrees of freedom to realize complex deformations of the soft body for self-propulsion at small scales (Figure 3a). In addition, the locomotory gait of the swimmer is not predefined at the

Palagi et al.<sup>[53]</sup> demonstrated the versatile locomotion of biomimetic swimming microrobots using photoactive LCE driven by structured dynamic light fields. The body of the LCE microrobot acts virtually as a continuum array of many infinitesimally small actuators, each of which can be independently triggered by the

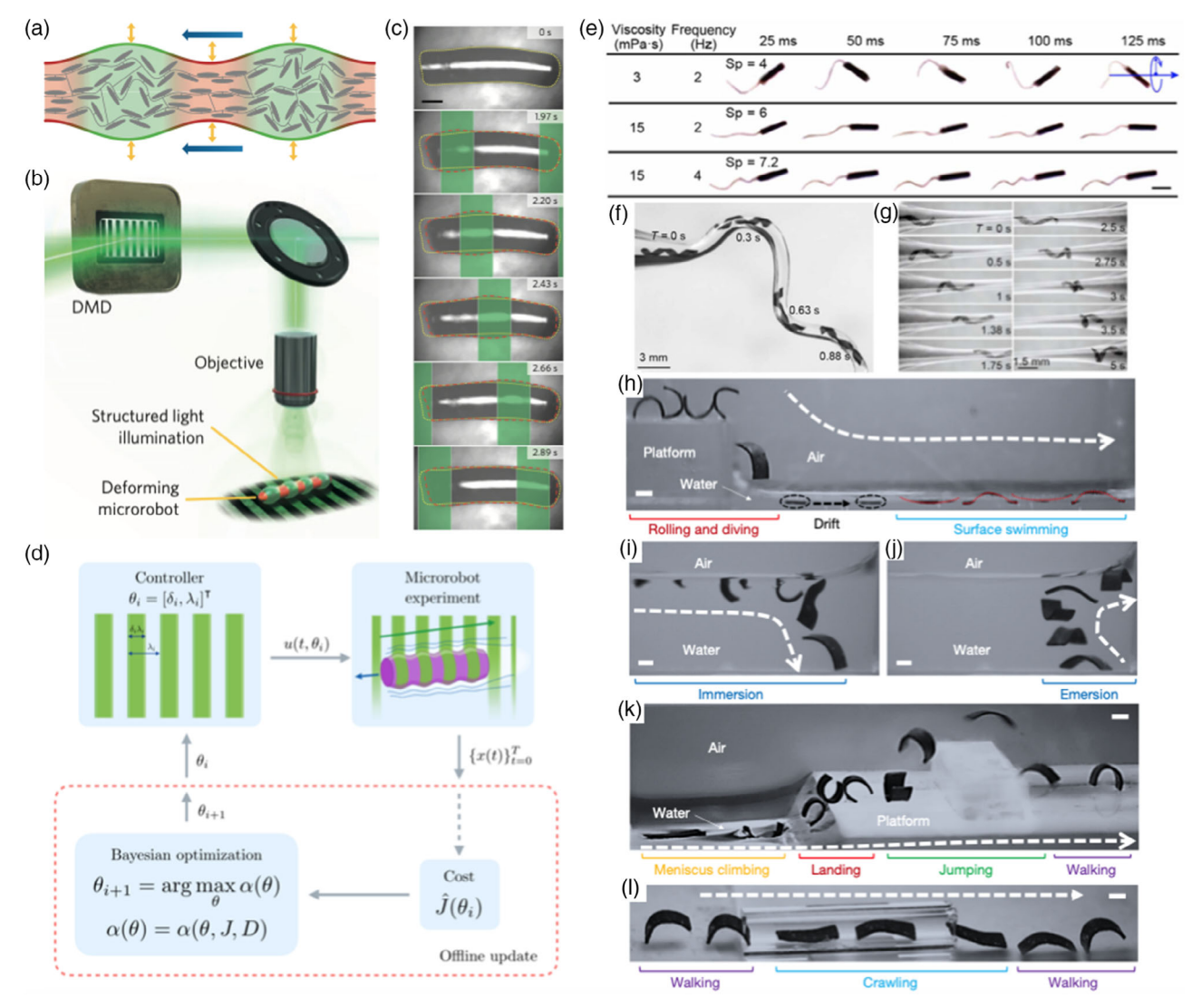


Figure 3. Exploiting soft active materials for adaptive locomotion. a-d) Light-driven soft microrobots. a-c) Reproduced with permission. [53] Copyright 2016, Macmillan Publishers Limited. d) Reproduced with permission. [62] Copyright 2018, IEEE. a) Selective deformation of a soft continuous microswimmer via photoresponse of LCEs under structured light fields. b) The structured light fields are generated by an optical systems based on a digital micromirror device (DMD). c) Experimental images (top-view) of an anchored cylindrical microswimmer deforming under a periodic light pattern traveling from left to right; illuminated areas are represented by the green overlay. Scale bar, 200 µm. d) Gait learning for light-driven soft microswimmers as cost-minimization problem over a parametric controller via Bayesian optimization (BO) with Gaussian Processes (GPs). The control input is the dynamic light field parameterized by  $\theta_i$ . In each iteration i, the controller generates the input signal u(t) that drives the microrobot, whose trajectory  $\{x(t)\}_{t=0}^T$  is tracked experimentally. The performance is evaluated by a cost function, which is given back to the optimizer and added to the dataset D. Given the posterior GP, BO suggests a new set of parameters for the next experiment by maximizing the acquisition function  $\alpha$ . e-g) Microswimmers exploiting elastohydrodynamic coupling for gait adaptation. Reproduced under a Creative Commons Attribution License (CC BY 4.0). [59] Copyright 2019 The Authors, some rights reserved; exclusive licensee American Association for the Advancement of Science. e) Optical images of microswimmers with shape-shifting tails moving at varying viscosities and rotating frequencies. Scale bar, 500 µm. f) Optical images of a flexible helical microswimmer passing through a highly curved microchannel under an externally applied flow (flow rate = 2 mL min<sup>-1</sup>). g) Shape change of filaments driven by velocity gradients in a cylindrical channel with a constriction (flow rate = 5 mL min<sup>-1</sup>). h–l) Multimodal locomotion of a magnetoelastic millimeter-scale soft robot over a hybrid liquid–solid environment. Reproduced with permission. <sup>[61]</sup> Copyright 2018, Macmillan Publishers Limited. These soft robots can switch between different locomotive modes and transit reversely between different liquid and solid terrains, including swimming inside and on the surface of liquids (h, i, j), climbing liquid menisci, rolling and walking on solid surface, jumping over obstacles (k), and crawling in narrow tunnels (l). Scale bars, 1 mm.



www.advintellsvst.com



fabrication stage but dynamically controlled through different light fields (Figure 3b). Such versatility allows the swimmer to be reconfigured in real time for adaptable locomotion behaviors. Based on the photoresponse of LCE to structured light, the researchers realized artificial microswimmers that self-propel by generating traveling-wave motions, closely mimicking the propulsion of micro-organisms (e.g., metachronal waves in ciliates)<sup>[13,63]</sup> (Figure 3c). The traveling-wave motion was induced by illuminating spatially periodic patterns of light and dark stripes that propagate along the swimmer's body.

This light-based approach provides refined spatiotemporal coordination required for adaptable locomotion behaviors, achieving a variety of swimming gaits with a single microswimmer. However, successful biomedical applications of this light-based approach may be constrained by limited penetration of light into biological tissues. The capability to generate structured light fields with refined resolution within the tissue remains a challenge to be resolved for in vivo applications (see also Section 3). Further development in bioimaging of live tissue, such as wavefront shaping methods<sup>[64]</sup> or advances in the use of near-infrared for deep imaging,<sup>[65]</sup> are required to bring these light-based strategies closer to in vivo applications.<sup>[66]</sup>

## 2.1.2. Gait Adaptation by Elastohydrodynamic Coupling

Huang et al. engineered magnetically powered microswimmers using origami design principles<sup>[58,59]</sup> (Figure 3e-g). The selffolding microswimmers were designed from a thermoresponsive gel reinforced with magnetic nanoparticles, where morphology and magnetization profile of the swimmers could be programmed. [58] Compliant microswimmers with self-regulation of motility and maneuverability were further developed.<sup>[59]</sup> The propulsion efficiency of these compliant swimmers depends on the coupling between magnetic forces, filament flexibility, and viscous drag. The elastohydrodynamic coupling enabled the swimmers to trigger a gait transition in response to changes in viscosity. Swimmers with tubular bodies and planar tails swam with an oar-like propulsion strategy at low viscosity and performed corkscrew motion at high viscosity due to coiling of the flexible tails (Figure 3e). This morphological transformation enhanced the swimmer's motility at high viscosity. These compliant swimmers could be programmed to reconfigure between a tubular body with a planar tail and a helical morphology, which performed better in a low viscosity fluid and a high viscosity fluid, respectively. Therefore, the swimmers with programmed shape change displayed both robust propulsion speed and enhanced maneuverability across varying fluid viscosity. Moreover, swimmers with helical shapes were shown to be able to adapt their shapes in response to complex geometric confinement and flow velocity gradient. The helical swimmer could bend its shapes to pass through a highly curved conduit under an external flow (Figure 3f) and elongated its axial length to pass through a conduit with a constriction (Figure 3g). All these shape transformations were elastic, and the swimmers recovered afterward, demonstrating elastohydrodynamic coupling as a mechanism for gait adaptation in traversing complex and dynamically changing environments.

## 2.1.3. Multimodal Locomotion of Magnetoelastic Soft Robots

Hu et al.<sup>[61]</sup> developed a magnetoelastic soft millimeter-scale robot that realized multimodal locomotion (Figure 3i-l). The potential of programming magnetic soft matter to achieve desired time-varying shapes has been demonstrated in an earlier work by Lum et al. [60] The robot was made of silicone elastomer embedded with hard magnetic neodymium-iron-boron microparticles and was programmed to have a single wavelength harmonic magnetization profile along its body. Through the interaction between a time-varying magnetic field and the magnetization profile, the robot could be controlled to change into different shapes and generate different modes of locomotion. A weak magnetic field caused a small deformation of a rectangular-sheet-shaped robot into a sinusoidal shape. Conversely, a strong magnetic field deformed the robot into a large-deflection shape of either a "C" or a "V" shape. By controlling the magnitude and the rotation of the magnetic field, the robot could perform multimodal locomotion in different environments. For example, the robot generated a swimming gait similar to that of a jellyfish by alternating between the "C" and "V" shapes. The robot could make use of its shape-changing mechanism under a time-varying magnetic field to transit reversely between liquid and solid terrains with different locomotion modes. The robot could swim inside liquids and swim on their surfaces (Figure 3i-j). It could also roll, walk, crawl, and jump on solid surfaces as well as climbing air-liquid interface of menisci (Figure 3k-l). These versatile modes of locomotion also enabled the robots to perform cargo pick up, transport, and release, demonstrating their vast potential toward medical applications. Although these millimeter-scale soft robots are larger than other microswimmers discussed in this Report, they are among the first to demonstrate adaptive locomotion across both liquid and solid terrains. These recent progresses call for further investigations into the possibility of scaling down these soft robots to the submillimeter scale.

## 2.2. Designing Adaptive Locomotion

While the use of soft active materials allows a large number of DOFs to be controlled for adaptive locomotion, another key challenge is to find effective locomotory gaits in different environments. Hand-tuning a large set of parameters is inefficient, time-consuming, and ineffective for varying, complex environments (see also Section 1.2). It becomes an even bigger challenge when there is no accurate locomotion model for the microrobots, or when uncontrolled factors arising from the fabrication of the microrobots and noises from their surrounding environments are present. We report the recent progresses mentioned in the following paragraphs on applying different gait learning approaches in realizing adaptive microswimmers.

#### 2.2.1. Gait Learning as a Parametric Controller Tuning Problem

Rohr et al.<sup>[62]</sup> presented a path toward self-adaptive microswimmers via a probabilistic learning approach to find effective locomotory gaits for a given environment (Figure 3d). Photoactive microswimmers<sup>[53,67]</sup> (see discussion in Section 2.1) were used as

www.advintellsvst.com

the model system, where parameters of periodic light patterns is tracked by real-time microscopy to obtain the state, reward or (e.g., size of the dynamic light and dark stripes and their gaps penalty as inputs to the learning algorithm. The extension of the in between) represent the control input in a parametric controller learning process to multiple swimmers also suggests the benefit tuning problem. The optimization takes place in the parameter of sharing information between multiple swimmers in speeding space of the light patterns with a specific cost function. Learning up the learning process. This work is among the first to implean optimal gait thus amounts to finding an optimal control input ment reinforcement learning with a microscale experimental platform in a real-world environment, via the integration with that minimizes the cost function. To account for uncertainties a computer and microscopy setup. It demonstrates the feasibility (e.g., in measurements and state estimation of the microand vast potential of the machine learning approach in the develswimmers), the cost function was modeled as a Gaussian process. In each learning trial for a given controlled input, the dynamics of opment of microswimmers. the swimmer was experimentally tracked and evaluated by the cost function. The gait performance was then optimized by the method of Bayesian Optimization, [68] which maximizes an acquisition function that determines the next state to evaluate.

#### 2.2.2. Reinforcement Learning of Microswimmers

Reinforcement learning<sup>[69]</sup> offers an alternative machine learning approach to designing adaptive locomotion of microswimmers. In this approach, the reinforcement learning agent learns to select actions given the states based on its experience interacting with the environment (Figure 4a). When performing each action in the environment, the agent obtains a numerical reward that measures the success of the action relative to the overall goal. Through the reinforcement learning algorithm, the agent will progressively learn to perform actions that maximize the cumulative reward in a certain application. We discuss three recent applications of reinforcement learning to microswimmers in the following paragraphs, which are all based on the Q-learning algorithm. The standard Q-learning algorithm is known for its simplicity and expressiveness, where the experience gained by the microswimmer is stored in a Q matrix, an action-value function that captures the expected long-term reward for performing the action given the state.<sup>[69]</sup>

This learning process then informed a new set of controller input

for the next trial. This gait learning approach resulted in a 115%

improvement in the locomotion performance of a microrobot,

demonstrating the possibility of realizing self-adaptivity with

light-based microswimmers and probabilistic learning control.

The first example is concerned with the gravitactic response of swimmers in the presence of complex flows, which presents a challenging flow navigation problem for artificial microswimmers. Colabrese et al. [70] have used *Q* learning to develop smart gravitactic swimmers with effective escape strategies to avoid being trapped by flow structures. With the ability to obtain partial information about its local surrounding flow and the use of *Q* learning, a smart gravitactic swimmer can learn nearly optimal strategies to swim upward by exploiting the underlying flow, based on its experience interacting with the environment (Figure 4b,c). This work demonstrates the vast potential of reinforcement learning in designing smart swimmers with adaptive behavior in complex environments.

The second example considers the navigation of active particles in a gridworld to target destinations (Figure 4d–f).<sup>[71]</sup> Implemented through *Q* learning, the system learns the policy to apply heat to specific positions on the particle with laser light to navigate the particle via self-thermophoresis from different starting cells to the target cell (Figure 4f). The swimmer position

More recently, Tsang et al.<sup>[72]</sup> considered a canonical swimmer model as an example to illustrate the use of reinforcement learning for designing locomotory gaits at low Re (Figure 4g-i). The model swimmer consists of an assembly of spheres connected by extensible rods (Figure 4g). Similar reconfigurable systems have been used to generate self-propulsion at low Reynolds numbers. [73–76] Unlike these traditional approaches where the swimming strokes were specified, here the spheres will self-learn propulsion policies based on knowledge gained by interacting with the surrounding medium via a reinforcement learning algorithm. Implemented via the Q learning algorithm, a self-learning swimmer can recover a previously known propulsion strategy (the Najafi–Golestanian's swimmer<sup>[73]</sup>), identify more effective locomotory gaits when the number of spheres increases, and adapt its locomotory gaits in different (e.g., viscous and frictional) media (Figure 4h-i).

These recent applications demonstrate the possibility of leveraging the prowess of machine learning to designing the next generation of smart microswimmers with adaptive locomotive capabilities.

Finally, despite significant recent progresses on adaptive locomotion, these algorithms and in vitro experiments remain in the proof-of-concept phase. In bringing them closer to in vivo applications, bioimaging becomes a major hurdle.<sup>[77]</sup> Refined resolution and sensitivity are required in realizing these adaptive locomotion strategies inside the human body, calling for further development in bioimaging techniques and integration with microscale systems.

#### 3. Tactic Artificial Swimmers

Swimming micro-organisms sense environmental stimuli and exhibit various tactic strategies to achieve biological goals. For example, chemotaxis is exhibited by bacteria to locate their nutrient rich environments<sup>[11]</sup> and by sperm cells to find the egg.<sup>[78]</sup> Phototactic micro-organisms swim and adapt in response to light conditions for optimal photosynthesis.<sup>[79,80]</sup> Apart from these tactic strategies, natural micro-organisms also respond to other external stimuli such as fluid flows, magnetic field, and gravity and adjust their motility accordingly.<sup>[81–83]</sup> This ability of adapting motions in response to external fields is crucial for effective navigation in biological fluids. Taking inspiration from nature, researchers have designed different artificial microswimmers that are capable of mimicking the tactic behavior of natural microswimmers and execute specialized tasks in complex environments.

Extensive efforts in the past decades have equipped artificial microswimmers with different types of tactic behaviors. Chemotaxis and magnetotaxis are among the most studied tactic

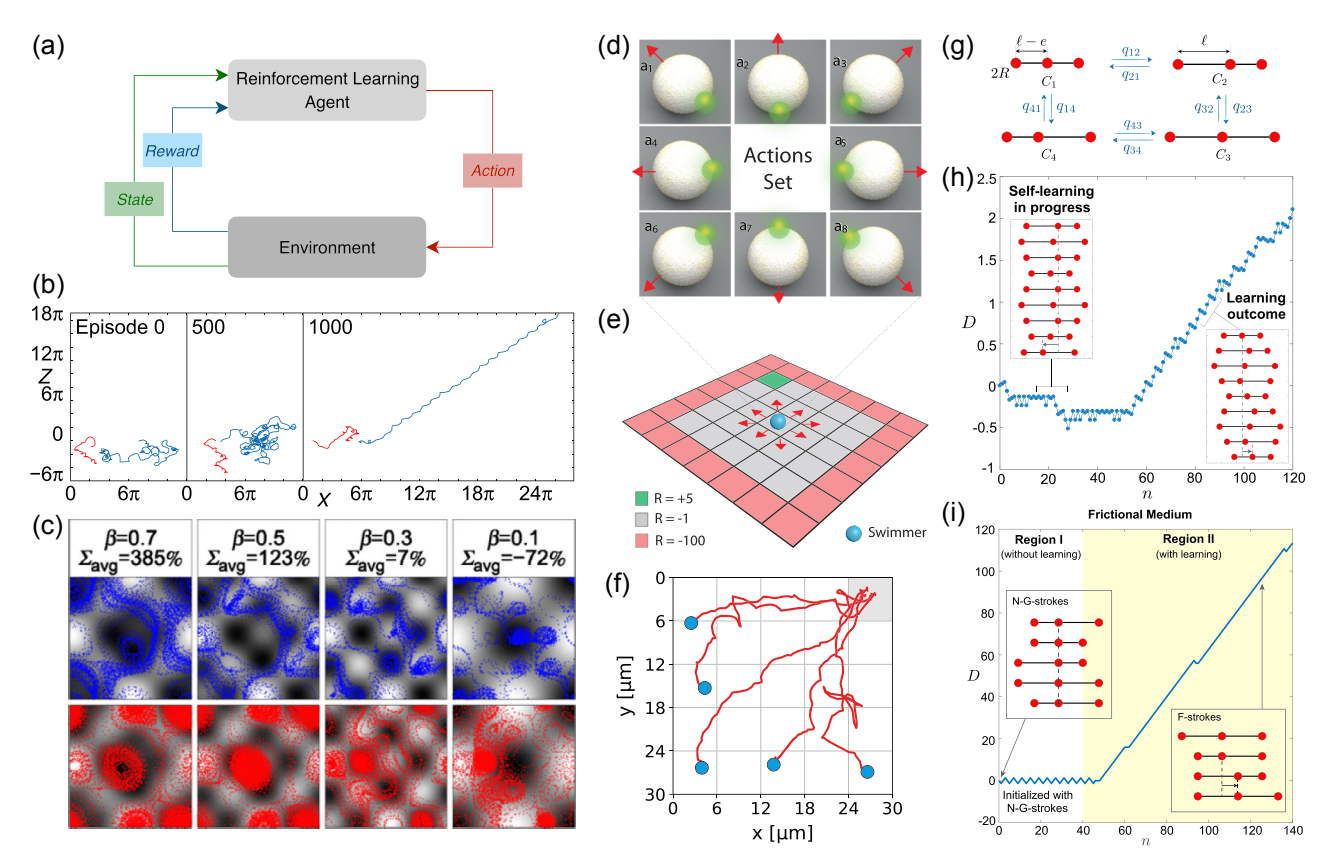


Figure 4. Reinforcement learning of microswimmers. a) Reinforcement learning enables an agent (e.g., smart swimmer) to learn by interacting with an environment. The reinforcement learning agent learns from the consequences of its actions, which are numerical rewards that encode the success of the actions relative to the goal. The agent progressively learns to select actions that maximize the cumulative reward in a particular application. [69] b,c) A smart gravitactic particle learns the best way to navigate and exploit the underlying complex flow to reach the highest attitude. Reproduced with permission.<sup>[70]</sup> Copyright 2017, American Physical Society. b) Comparison of representative trajectories at different learning episodes for smart gravitactic particles (blue) and typical trajectories for naive gyrotactic particles (red) in a Taylor-Green vortex flow and c) perturbed flows. The parameter  $\beta$  controls the intensity of the perturbation ( $\beta$ =1 corresponds to the original training environment), and  $\Sigma_{avg}$  denotes the averaged learning gain, which measures the relative increase in the return for smart gravitaxis relative to the return for naive gyrotaxis. d-f) Navigation of self-thermophoretic active particles in a gridworld to reach a target destination. Reproduced with the permission of the authors. [71] d) The actions are conducted by setting a specific heating position on the circumference of the particle, defining the propulsion direction. e) The sample region is coarse-grained into a gridworld of 25 states, where each cell represents a state. The swimmer transits between different states by executing different actions, collecting rewards (R) that can be positive or negative as indicated in the legend. f) Typical trajectories for the swimmer starting at different states reaching the target destination (gray cell) after the learning process. g-i) Self-learning locomotory gaits to swim at low Reynolds number via Q learning. [72] g) A simple reconfigurable system consisting of three spheres connected by two extensible rods. For a given configuration of the swimmer (the state) in a learning step, the swimmer could extend or contract one of its rods (the action) to transforms from the current state to a new state. Such an action resulted in a displacement of the swimmer's body centroid (the reward), which measures the immediate success of the action relative to its goal. Here  $q_{ij}$  represent entries in the Q matrix that evolve based on reinforcement learning. h) A typical learning episode of a three-sphere swimmer in a viscous fluid, where n is the number of learning step and D represents the cumulative swimmer displacement (dimensionless). The swimmer has no prior knowledge of low Reynolds number swimming but self-learns how to swim based on its interactions with the surrounding viscous fluid environment. The learning outcome recovers the Najafi-Golestanian's swimming strokes (N-G strokes).[73] i) Gait adaptation in a frictional medium. The N-G strokes (left inset) fails to propel in the frictional medium (region I) due to the absence of hydrodynamic interaction. When the learning algorithm is turned on, the self-learner rapidly identifies new effective locomotory gaits (F strokes, right inset) to propel in the frictional medium (region II).

behaviors for artificial microswimmers, with relatively solid theoretical foundation and abundant experimental implementations. However, in vivo medical applications are still limited with concerns on the biocompatibility and toxicity of these synthetic structures, especially for chemical swimmers which usually involve the use of toxic chemical fuels. Recently, in vitro experiments on phototactic and rheotactic artificial swimmers have demonstrated promising results as proof of concept, but their

applicability in realistic in vivo environments remains to be addressed. Finally, studies on gravitaxis and viscotaxis for artificial microswimmers are still at their early development stage. In particular, most recent efforts on artificial viscotactic swimmers remain theoretical, which calls for experimental implementation. Below, we survey these recent developments in more detail and discuss promising directions in addressing outstanding challenges for in vivo medical applications.

#### ADVANCED INTELLIGENT SYSTEMS

#### 3.1. Chemotaxis

Chemotaxis, the response to chemical gradients, allows bacteria to move toward or away from a particular chemical attractant or repellent by biased random walks through altering the tumbling frequency. [11] Artificial microswimmers such as catalytic Janus particles can also imitate chemotaxis but with qualitatively different mechanisms than biological swimmers. [84-87] These catalytic Janus particles can swim by self-diffusiophoresis, where self-generated chemical gradients due to reactions at the particle surface lead to phoretic motion of these particles.<sup>[39]</sup> When there are nonuniform concentration fields, the fluid flows set up around the Janus particle can reorient the particle's symmetry axis in response to local gradients of the substrate concentration<sup>[84,86,87]</sup> (**Figure 5**a). In the presence of nearby particles, their chemotactic interactions were shown both theoretically and experimentally to display a rich array of collective behaviors, including for formation of dynamic clusters, asters, and wave patterns<sup>[84,87,88,90–93]</sup> (Figure 5b). Previous studies also demonstrated the chemotaxis of droplet swimmers in different chemical systems, [94–96] guiding the droplets through microfluidic maze (Figure 5c-e) and branch selection by autochemotactic signaling. [89] As a remark, the biohybrid approach, which exploits the locomotion and tactic behaviors of living cells, such as neutrophils, sperm cells, or bacteria, [97-99] could lead to more effective carriers for specific drug delivery or fertilization-related problems. [99-101] Nevertheless, purely artificial chemotactic machines offer alternative strategies in biomedical applications when there are concerns on specificity or pathogenicity of the biohybrid approach. Yet, concerns on the biocompatibility of artificial structures and toxicity in chemical-based strategies will also need to be addressed. [102-104] An important next step is to examine the applicability of these artificial tactic strategies in in vivo biological environments. As an example, recent experiments have demonstrated that chemotaxis of self-propelling vesicles (polymersomes) in the presence of glucose gradients can enable a fourfold increase in delivery across the blood–brain barrier compared with nonchemotactic systems. [105] In addition to their biomedical uses, purely artificial chemotactic machines find potential applications in environmental damage remedies, such as locating the source of pollution and decomposing the pollutants into harmless products. [101,106]

#### 3.2. Magnetotaxis

The motion of some micro-organisms (e.g., magnetotactic bacteria[107,108]) is guided by magnetic fields due to the presence of organelles containing magnetic nanoparticles called magnetosomes, which act as compass needles for navigation along the magnetic field. Similarly, for artificial microswimmers driven by external magnetic fields<sup>[8,9,35,109]</sup> or hybrid motors consisting of magnetic components, [110,111] the constituting magnetic material allows the steering of the microswimmer through adjusting the external magnetic field. Swimmers that are not magnetically driven (e.g., swimmers that propel by bubble generation or selfphoretic particles), can be guided by magnetic fields through the incorporation of magnetic materials into the swimmers. This method includes the addition of nickel segments, [112-114] iron or iron-based objects<sup>[115–117]</sup> into rod-like (Figure 6a) or tabular (Figure 6b-d) motors. However, these approaches, which rely on the magnetic shape anisotropy of the rod-like and tabular structures, are difficult to apply to spherical Janus motors due to their symmetry. Baraban et al. [118] designed spherical Janus particles combining catalytic and magnetic cap structures, where the magnetic moment is aligned along the main axis of symmetry of the cap by the deposition of ultrathin magnetic multilayer films onto the spheres (Figure 6e). More recently, manganese ferrite nanoparticles have been coated on spherical, double-fueled Janus

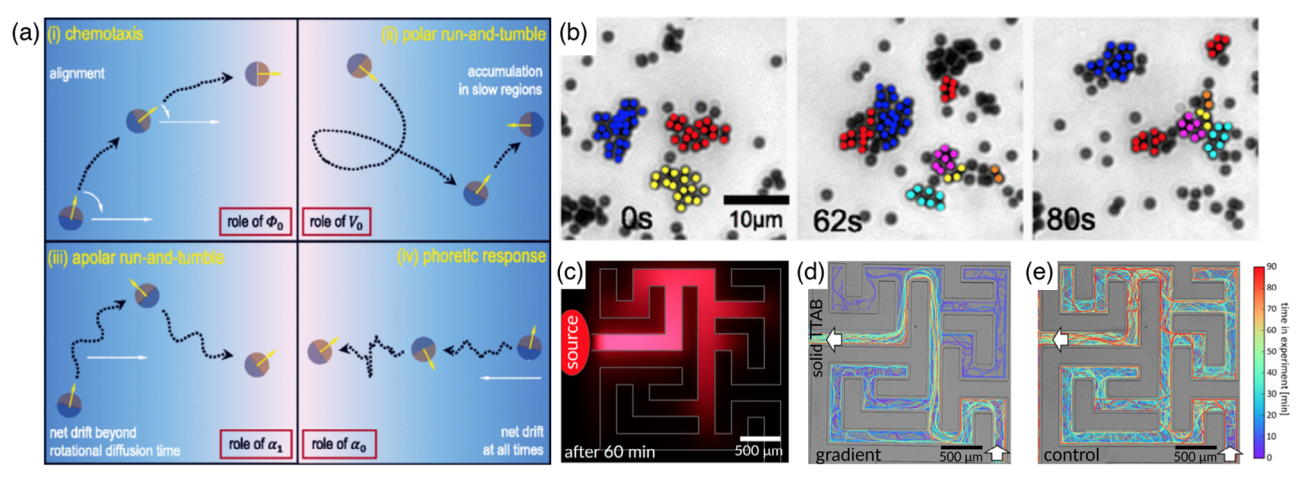


Figure 5. Chemotaxis of artificial microswimmers. a) Schematics illustrating different ways a single phoretic swimmer responds to chemical gradients [(i)–(iv)], depending on details of geometry, activity, and mobility of the particle. Reproduced with permission.<sup>[84]</sup> Copyright 2014, American Physical Society. b) Emergence of dynamic clustering in active colloidal suspensions with chemical signaling. Reproduced with permission.<sup>[88]</sup> Copyright 2012, American Physical Society. c–e) Maze solving by chemotactic droplet swimmers. Reproduced with permission.<sup>[89]</sup> Copyright 2017, National Academy of Sciences of the United States of America. c) Distribution of ionic surfactant, tetradecyltrimethylammonium bromide (TTAB), mixed with fluorescent Nile Red in the maze after 60 min, with the point of release marked as "source." Trajectories of swimmers in the maze with (d) and without (e) TTAB gradient. Line colors correspond to the time in the experiment.

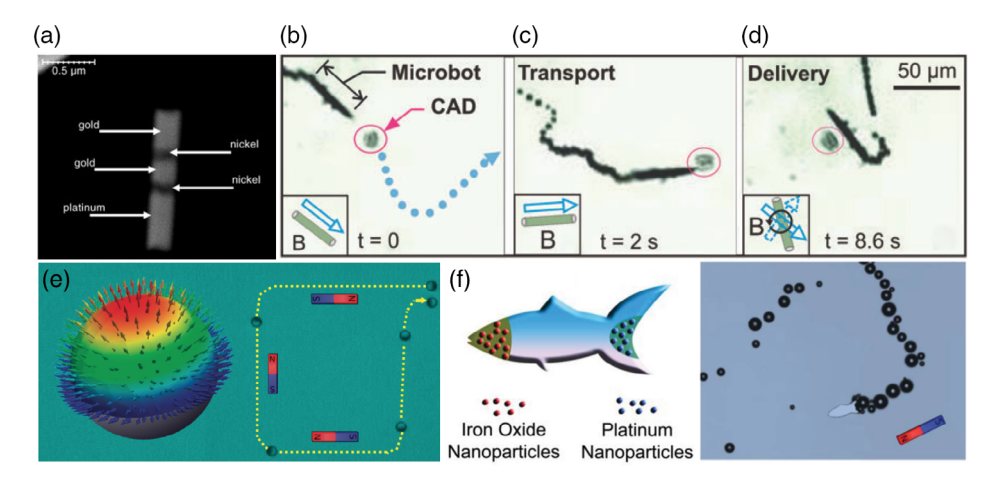


Figure 6. Magnetotaxis of artificial microswimmers. a) A scanning electron microscopy image of a striped metallic nanorod with Pt, Ni, Au, Ni, and Au segments. The Pt segment catalyzes the decomposition of hydrogen peroxide and the ferromagnetic nickel segments can be magnetized for controlling the direction of the rod. Reproduced with permission.[112] Copyright 2005, Wiley-VCH, b-d) Controlled manipulation of CAD cells (cathecolaminergic cell line from the central nervous system) by Ti/Fe/Pt microtubes. The motion of the catalytic microbot is aligned by an external magnetic field (insets). Reproduced with permission. [115] Copyright 2011, The Royal Society of Chemistry. e) Catalytic Janus motor combined with magnetic cap, where the resulting magnetic moment is aligned along the main axis of symmetry of the cap. The catalytic and magnetic cap structures allow the Janus motor to be guided by an external magnetic field. Reproduced with permission. [118] Copyright 2012, American Chemical Society, f) Schematic illustration of a microfish loaded with Pt nanoparticles for catalytic propulsion and Fe<sub>3</sub>O<sub>4</sub> nanoparticles for magnetic control (left); the microfish's movement can be guided magnetically (right). Reproduced with permission. [119] Copyright 2015, Wiley-VCH.

swimmers. [120] Iron oxide nanoparticles have also been loaded into 3D-printed fish-like catalytic microswimmers for magnetic control<sup>[119]</sup> (Figure 6f). In addition to chemical swimmers, ultrasound-propelled nanowire motors with embedded nickel segments can also facilitate magnetically guided motion as well as transporting large cargo along predetermined paths.[121] Finally, we remark that the biohybrid approach, which integrates either the self-propelling or the magnetotactic capabilities of micro-organisms with artificial structures, offers an array of biohybrid microrobots. We refer the readers to specialized reviews on this biohybrid approach.[25-30,122]

## 3.3. Phototaxis

Phototactic behavior allows motile photosynthetic microorganisms to move either toward the light source to receive more energy for photosynthesis or away from it to avoid exposure to damaging radiation. Artificial microswimmers capable of sensing the external light source and orienting to it enable additional control of their direction of motion and optical navigation in healthcare applications, such as noninvasive surgery and drug delivery. Dai et al. [123] designed a phototactic microswimmer with a Janus nanotree structure (an array of titanium dioxide, TiO<sub>2</sub> nanowires grown on a silicon nanowire, **Figure 7**a). These light-driven microswimmers propel by self-electrophoresis, where the asymmetrically distributed ions along the nanotree are generated by the photoelectrochemical (PEC) reaction. The phototactic behavior stems from the different PEC reaction rates between the illuminated and shaded side of the TiO2 nanowires. The difference results in an unbalanced charge distribution, which generates an electric field parallel to the propagation direction of the light and hence a torque that reorients the swimmer in response to the light source. In more recent experiments, Zheng et al. [124] coded microswimmers with distinct spectral responses by loading the nanotrees with different dyes. Such coding enables independent navigation of multiple dye-sensitized microswimmers (Figure 7b).

Light-driven self-diffusiophoretic particles, such as optically transparent silica spheres capped on one side with a lightabsorbing carbon layer<sup>[125]</sup> and carbon-nitride-coated platinum particles, [126] can also display phototactic response to light gradients, similarly due to the dependence of chemical activity of the particle surface on the local light intensity (Figure 7c). Recent experiments have demonstrated photogravitactic behaviors for light-driven self-diffusiophoretic particles, [127] where these particles lift-off from wall and swim away from the light source against gravity above a certain light intensity threshold.

Light fields are readily adjustable spatially and temporally, which makes the light-based approach appealing for dynamic environments. [53,125] However, potential restrictions on healthcare applications of these phototactic strategies include the challenge of light penetration into biological tissues (see also Section 2.1) and harmful effects stemming from the choice of illumination (e.g., ultraviolet [UV] radiation). The development of optical techniques such as wavefront shaping may enable the penetration of tightly focused light deep into biological tissues. [64] Further investigations on the choice of photoactive materials may also allow harmful UV radiation to be replaced by biocompatible visible or infrared illumination. [123]

#### 3.4. Rheotaxis

Biological and artificial swimmers often encounter external fluid flows. Rheotaxis is a form of taxis observed in many aquatic

www.advintellsvst.com

www.advancedsciencenews.com

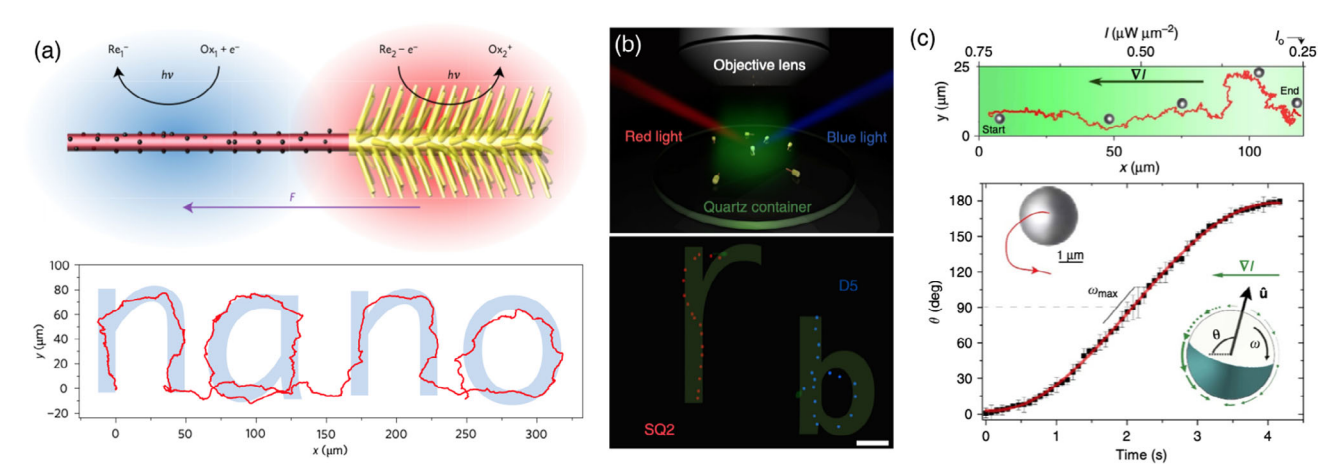


Figure 7. Phototaxis of artificial microswimmers. a) Top: schematic of a Janus self-electrophoretic microswimmer, consisting of an array of TiO2 nanowires (yellow) grown on a silicon nanowire (pink). Reproduced with permission. [123] Copyright 2016, Macmillan Publishers Limited. Bottom: Navigated by light, the trajectory of the phototactic swimmer spells "nano." b) The orthogonal orientation control and navigation of dye-sensitized microswimmers. Reproduced under a Creative Commons Attribution License (CC BY 4.0). [124] Copyright 2017, The Author(s), Published by Springer Nature, Top: the blue and red lights are used to control the orientation of the microswimmers, whereas the green light is used for imaging. Bottom: navigated by the blue and red lights, the trajectory of red- and blue-sensitized microswimmers spell, "r" and "b," respectively (scale bar: 20 μm). c) Phototaxis of self-diffusiophoretic particles. Reproduced under a Creative Commons Attribution License (CC BY 4.0). [125] Copyright 2016, The Author(s). Published by Springer Nature. Top: trajectory of a phototactic, self-diffusiophoretic particle in a constant light gradient  $\nabla I$ . Bottom: time evolution of the orientation angle  $\theta$  of the swimmer. Lower inset: The axially asymmetric slip velocities (green arrows) result in an angular velocity  $\omega$  and hence the reorientation.

organisms, which allows them to respond to external flows to facilitate different biological functions, such as accessing food, migration, and for sperm cells to reach the egg.[128] Palacci et al.[129] demonstrated artificial rheotaxis with an anisotropic active particle consisting of a spherical body of 3-methacryloxypropyl trimethoxysilane polymer and a hematite cube protruding out from the particle surface (Figure 8a). The rheotactic behavior originates from the alignment of the active polar particle with the flow (Figure 8b,c), where the particle experiences a viscous torque under a shear flow and migrates upstream (positive rheotaxis). More recently, Ren et al.[130] designed bimetallic microrods which exhibit not only positive rheotaxis based on the same mechanism as the hematite swimmers, [129] but also negative rheotaxis by combining the chemical orientation mechanism with directional propulsion using the acoustic field. The direction of rheotaxis can be selected depending on the composition of the bimetallic rods (Figure 8d-e). As a remark, analytical and numerical calculations suggested that under certain conditions rheotaxis can also occur for active particles without shape anisotropy (e.g., spherical catalytic Janus particles) due to the near-wall swimming activity of the particle. A recent study has shown through experiments and simulations how to tune rheotactic response by controlling the distribution of surface slip.<sup>[131]</sup> Building on these recent progresses, an important next step is to demonstrate the feasibility of these artificial rheotactic strategies in realistic biological scenarios relevant to their biomedical applications.

#### 3.5. Gravitaxis

Some motile micro-organisms can respond to Earth's gravity and orient themselves to swim upward. [132–134] Such orientation capability, termed negative gravitaxis, allows the microorganisms to counteract sedimentation and thus extend the range of their habitat. The gravitactic response could result simply from a purely passive mechanism due to asymmetric distribution of mass density in bottom-heavy cells. With a similar mechanism, Campbell and Ebbens<sup>[135]</sup> demonstrated artificial gravitaxis with spherical catalytic Janus swimmers (Figure 9a), whose orientations were biased toward the cap-down configuration with respect to gravity. Alternatively, Hagen et al. [136] showed that asymmetric shape (Figure 9b, e.g., L-shaped swimmers), alone, can also result in gravitactic response, either preferential upward or downward swimming. As a remark, we also discussed in Section 2.2, a theoretical approach in designing smart gravitactic active particles via reinforcement learning.<sup>[70]</sup> Most recent efforts are still in the stage of proof of concept, and the link to practical applications of artificial gravitaxis remains to be built.

## 3.6. Viscotaxis

While some micro-organisms are known to move up (e.g., Leptospira<sup>[139]</sup>) or down (e.g., E. coli<sup>[140]</sup>) the viscosity gradients, this type of tactic behavior—viscotaxis—is less understood compared with other types of taxes discussed earlier. Liebchen et al. [137] constructed model swimmers consisting of assemblies of spheres to demonstrate that viscotactic motion can emerge from an asymmetry of viscous forces on different parts of the swimmer (Figure 9c). These results hence suggest the association of dynamic body shape changes of micro-organisms with their viscotactic behaviors. More recently, Datt and Elfring<sup>[138]</sup> considered a spherical squirmer model to show that viscotactic response can also occur with axisymmetric squirmers (Figure 9d), which generally turn toward regions of lower

www.advintellsvst.com

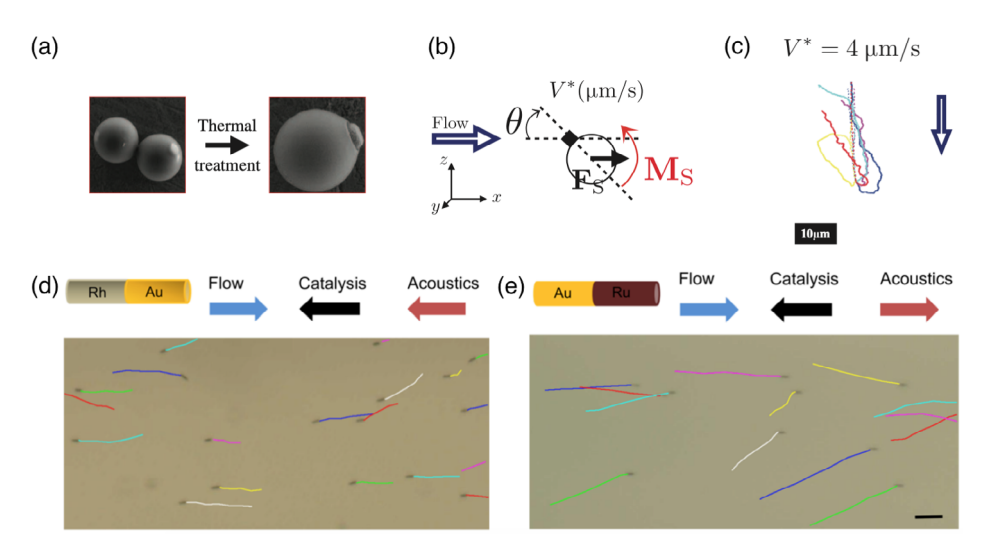


Figure 8. Rheotaxis of artificial microswimmers. a-c) Artificial rheotaxis with an anisotropic active particle driven by the photocatalytic decomposition of the hydrogen peroxide fuel by hematite. Reproduced under a Creative Commons Attribution License (CC BY 4.0). [129] Copyright 2015 The Authors, some rights reserved; exclusive licensee American Association for the Advancement of Science. a) A thermal treatment results in an anisotropic particle consisting of a spherical body of 3-methacryloxypropyl trimethoxysilane polymer and a hematite cube protruding out from the particle surface. b) A model assuming that the hematite component acts as a fixed pivot, linked to the substrate, with  $\theta$  denoting the angle between the tail-head direction of the particle with the flow. The flow exerts a viscous drag  $F_s$  on the body of the particle, resulting in a torque  $M_s$  that aligns the particle with the flow. The alignment combines with the polarity of the self-propulsion induces an upstream migration. c) Trajectories of the particles in the absence (dashed lines) and presence of (solid lines) of light under a flow. The flow direction is indicated by the blue arrow. In the absence of light, the particle acts as a passive tracer advected at velocity  $V^* = 4 \,\mu\text{m s}^{-1}$  under the flow. When activated by light, the particle self-propels at  $V_0 = 8 \,\mu\text{m s}^{-1}$  without an imposed flow. Under the external flow, the particle re-orients with the hematite protrusion facing the flow and hence migrates upstream. d,e) positive and negative rheotaxis of synthetic bimetallic micromotors via a combination of chemical fuel and acoustic force. Reproduced with permission. [130] Copyright 2017, American Chemical Society. d) For Rh-Au micromotors, the direction of their axial motion in the chemical and acoustic fields is the same. In the chemicalacoustic hybrid field, these micromotors exhibit positive rheotaxis. e) For Ru–Au micromotors, the direction of their axial motion in chemical and acoustic fields is opposite, and acoustic propulsion dominates the axial motion. These micromotors exhibit negative rheotaxis. Scale bar, 10 µm.

viscosity (negative viscotaxis). These studies lay the theoretical foundation for the development of artificial viscotactic microswimmers and strategies to sort and control these swimmers with the use of viscosity gradients, which may be generated by concentration or temperature difference. [141-143] Artificial viscotaxis is among the least studied type of tactic behaviors. These recent theoretical efforts call for experimental implementation and more practical considerations in terms of their biomedical and environmental applications.

## 4. Multifunctional Swimmers

In addition to robust locomotion across varying environments (Section 2) and navigating complex environments in response to external stimuli (Section 3), smart microswimmers need to be armed with additional functionalities to perform complex tasks for their biomedical or environmental applications. We highlight recent progress in designing multifunctional microswimmers in two areas as examples: 1) cargo manipulation and 2) multiswimmer operations in this section.

#### 4.1. Cargo Manipulation

In their applications in drug delivery, microswimmers can be used to transport therapeutic payloads to targeted locations. They can also be used to collect and transport biological samples from pathological sites for diagnostic purposes. Artificial helical propellers can manipulate cargo through direct contact (e.g., pushing and rotating<sup>[9,109]</sup>). To stabilize the loading and transport process, various strategies have been explored. [144] For instance, microswimmers with microholders can transport microparticles more stably due to lateral confinement from the protrusions of the microholder.[145,146] Magnetic attraction between the swimmer and the cargo was exploited.[113] Gao et al.[147] developed magnetic flexible swimmers to transport drug-loaded poly (lactic-co-glycolic acid) (PLGA) particles encapsulating iron oxide particles to HeLa cancer cells. The cargo pickup is enabled by the attraction between the magnetic head of the swimmer and the iron oxide particles inside the PLGA cargo. When the swimmer with the PLGA cargo is directed to approach the target cell, the cargo is not released; instead, the swimmer is nonspecifically bound to the cell to enable localized drug release from the cargo. Instead of picking up drug-loaded particles via magnetic attraction, magnetic microswimmers can also be functionalized with drug-loaded liposomes in advance. [148] For catalytic Janus motors, Baraban et al.<sup>[118]</sup> combined catalytic and magnetic cap structures to enable steering and cargo manipulation. Cargo release is realized by adjusting the magnetic field orientation. Electrostatic force or chemical interaction have also been used for self-assembly of the swimmers and surface functionalized cargos.  $^{[144,149]}$  More recently, with the aim of assisting fertilization,

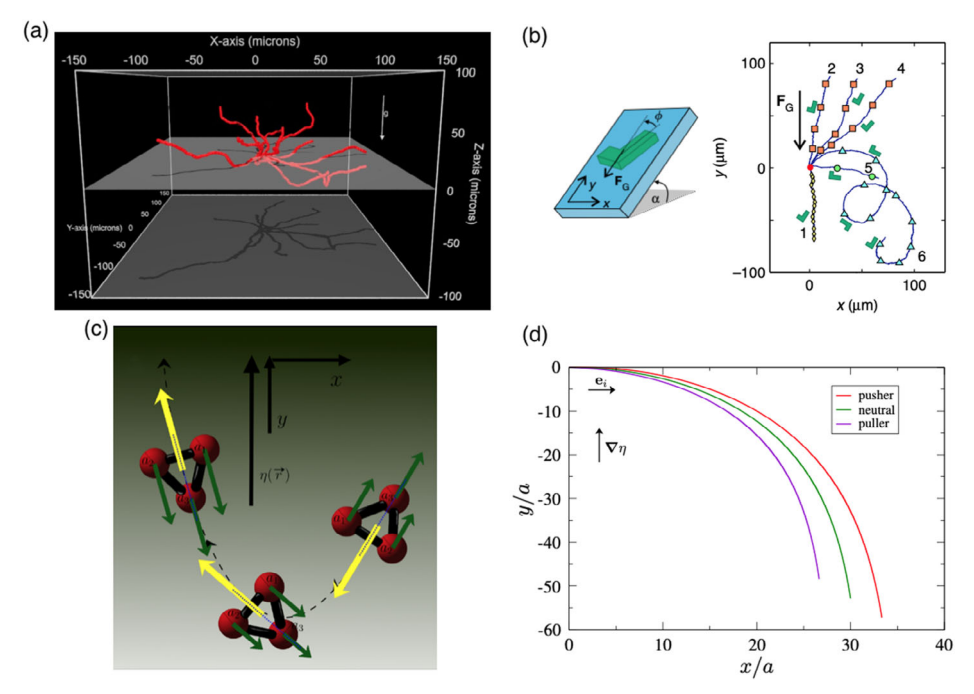


Figure 9. a,b) Gravitaxis and c,d) viscotaxis of artificial microswimmers. a) 3D swimming trajectories of catalytic Janus swimmers demonstrate gravitactic response due to the asymmetrical distribution of mass density at the surface of the swimmer. Reproduced with permission. [135] Copyright 2013, American Chemical Society. b) Swimmer with asymmetric shape (e.g., L-shaped swimmer) alone can induce gravitaxis. Reproduced with permission. [136] Copyright 2014, Macmillan Publishers Limited. Left: An asymmetric self-diffusiophoretic particle covered with a thin Au coating on the front side of the short arm. When the particle is suspended in a binary mixture of water and 2,6-lutidine at critical composition, laser illumination causes local heating and hence local demixing of the solvent, resulting in intensity-dependent phoretic propulsion. Right: Trajectories of the L-shaped swimmer, starting at the origin of the graph, under different illumination intensities. c) A mechanism for viscotactic behavior of a nonaxial swimmer in a nonuniform viscosity field  $\eta(\vec{r})$  based on a systematic asymmetry of viscous forces acting on a microswimmer. Here, the viscous drag on body parts at high viscosity (sphere 1) dominates the drag on spheres at low viscosity (sphere 2), turning the swimmer up the viscosity gradient. Reproduced with permission. [137] Copyright 2018, American Physical Society. d) Viscotactic response can also occur for axisymmetric squirmers (pushers, pullers, or neutral squirmers), which generally display negative viscotaxis. Reproduced with permission. [138] Copyright 2019, American Physical Society.

Medina-Sánchez et al. [150] used magnetic helical microswimmers to mechanically capture and transport sperm cells that cannot swim effectively toward the egg. The pickup and release of the cargo (sperm cell) is achieved by directing the microhelices toward (pick up) and away (release) from the sperm cell.

An alternative class of cargo manipulation methods involves the use of fluid flows generated by the microswimmer. [144,151–158] Depending on the type of swimmer and details of its actuation mechanism, the flow around an approaching swimmer may trap or push away the target cargo. In particular, the flow generated by a rotating microswimmer can be exploited for entrapment and release of cargo particles. [154–156,159] Recently, Huang et al. [160] combined a magnetic screw with an Archimedean screw pump to facilitate the loading and releasing of multiple microparticles (Figure 10a). In the loading process, an external magnetic field drives the rotating screw, which draws the microparticles into the cylinder with the fluid flow, whereas the piston slides forward to close the rear side of the cylinder and trap the microparticles within. In the releasing process, the screw is rotated in reverse, opening the cylinder and generating a reverse fluid flow to expel the trapped particles.

Recent efforts have also moved toward relying less on external manipulation and are capable of responding to external stimuli (physical, chemical, or biological). As we move closer to realistic

medical applications, biocompatibility, biodegradability, and recovering of swimmers after completing the tasks also become important design considerations. We note that extensive studies have exploited the use of biological cells to achieve these complex cargo manipulations. We refer the readers to comprehensive reviews on these biohybrid strategies<sup>[25-30,122]</sup> and focus on the development of artificial swimmers along these directions as given in following paragraphs.

For swimmers that are not of biological nature, researchers found ways of constructing biodegradable artificial swimmers. Bozuvuk et al. [161] 3D printed their swimmers using chitosan combined with superparamagnetic iron oxide nanoparticles to make it biodegradable and magnetically steerable at the same time (Figure 10b). Furthermore, they used a photocleavable chemical to deposit doxorubicin (a chemotherapy drug) onto the swimmer, which facilitates the light triggered release of the drug on demand. Light-triggered release of drug or cargo also applies to swimmers that are propelled by chemical means. For example, Sundararajan et al.[162] added a silver link between their catalytic Pt-Au nanomotor and the PS amidine cargo to exploit the rapid degradation of Ag molecules in the presence of hydrogen peroxide, chloride, and UV light, and thus achieved UV triggered, on demand release of the cargo (Figure 10c).



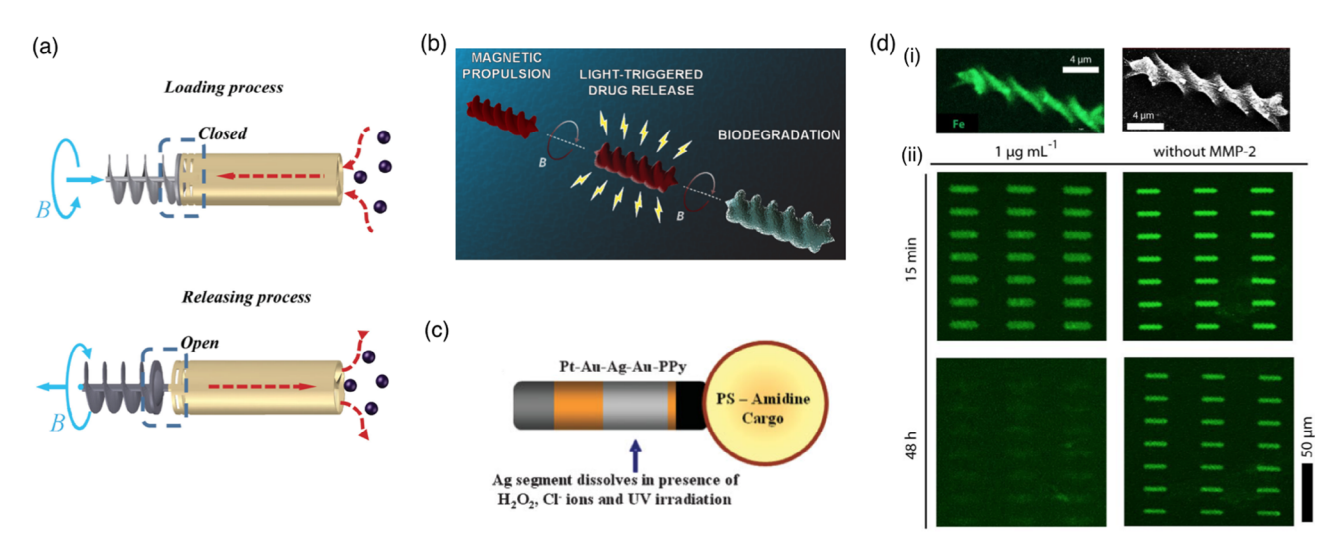


**Figure 10.** Cargo manipulation by multifunctional swimmers. a) Schematic illustration of a microtransporter that exploits fluid flow for entrapment and release of multiple microparticles. Reproduced with permission. Copyright 2015, Wiley-VCH. b) Light applied to the helical swimmer starts to decompose the swimmer and release the drug. Further application facilitates the complete biodegradation of the swimmer. Reproduced with permission. Copyright 2018, American Chemical Society. c) Hydrogen peroxide and chloride dissolve silver when subjected to UV light, breaking the link between the swimmer and the cargo, thus releasing the drug. Reproduced with permission. Copyright 2010, Wiley-VCH. d) i) Energy dispersive mapping is used to confirm that the iron particles are homogeneously dispersed in the swimmer body; ii) Left column depicts the perishing of the swimmers at high concentrations of MMP-2. Helical swimmers swell in the presence of MMP-2 enzyme and start decomposing. Drug is released from the destroyed swimmers. The magnetic particles deposited on the swimmer for propulsion, which are tagged with antibodies, find the remaining sick cells. Right column underlines the lack of disintegration in the absence of MMP-2. Reproduced with permission. Copyright 2019, American Chemical Society.

More recently, Ceylan et al.<sup>[163]</sup> designed a 3D-printed microswimmer that self-destructs while delivering its cargo as a response to pathological markers in its microenvironment. The hydrogel-based, enzymatically degradable microswimmer swells and decomposes at high concentrations of matrix metalloproteinase-2 (MMP-2) enzyme, whose overexpression is a potential biomarker for certain types of cancers such as colorectal cancer. Upon full degradation, the microswimmer not only releases the embedded therapeutic cargo molecule but also other functional cargos, such as anti-ErbB 2 antibody-tagged magnetic nanoparticle, for targeted labeling of cancer cells. This design combines the key functions of diagnosis, treatment, and follow-up of the disease on one swimming agent (Figure 10d).

## 4.2. Multiswimmer Operations

Practical applications of microswimmers could involve a large number of them to deliver sufficient dosages in drug delivery or perform multiple tasks in microsurgery. Diverse collective behaviors can emerge among different types of microswimmers. [15,164–166] The controllability of groups of microswimmers and their capability to perform complex operations are therefore essential to the next generation of smart microswimmers. Herein, we discuss some recent ideas on coordinated operations of purely artificial swimmers to allow for greater versatility. We remark that swarms of biological and biohybrid microswimmers can also be controlled for medical applications, [167–169] but we refer the readers to more specialized reviews on these topics. [26,29,122,170]

Assemblies of active particles (e.g., clusters of Janus catalytic particles) can display a variety of trajectories different from

individual active particles, depending on their specific configurations. [32,171] The capability for microswimmers to perform dynamic assembly and disassembly, instead of preassembled structures, enables reconfiguration of the assembly "on-the-fly" to display different propulsion behaviors. Gao et al. demonstrated dynamic assembly of Janus catalytic motors induced by hydrophobic surface interactions.[172] Although the change of assembly configuration and hence propulsion characteristics were demonstrated (Figure 11a), disassembly of the cluster may not be possible, and the assembly process requires more control. The dynamic assembly and disassembly processes are more controllable for magnetic helical microstructures, [173] which can be assembled into various configurations by adjusting the direction, speed, and strength of the rotating magnetic field (Figure 11b). The assembled swimmers with various configurations display different swimming characteristics, including the reversal of swimming directions. In addition to helical swimmers, Vach and Faivre<sup>[175]</sup> demonstrated the possibility of realizing different types of magnetic actuation (rolling, propelling, and swimming) with a single nanostructured magnetic material. The swimming mode requires individual particles to first undergo magnetically guided self-assembly into chainlike structures. Cheang et al.[174] also demonstrated modular microswimmers<sup>[176]</sup> consisting of magnetic microbeads assembled by magnetic attraction. Figure 11c shows controlled assembly from three-bead to nine-bead microswimmer (i-vi), as well as the disassembly of the nine-bead microswimmer into smaller subunits (vii) by adjusting the rotational frequency of the magnetic field. Microswimmers with different number of beads were shown to have varying swimming behavior. This modular approach offers additional versatility for navigating diverse

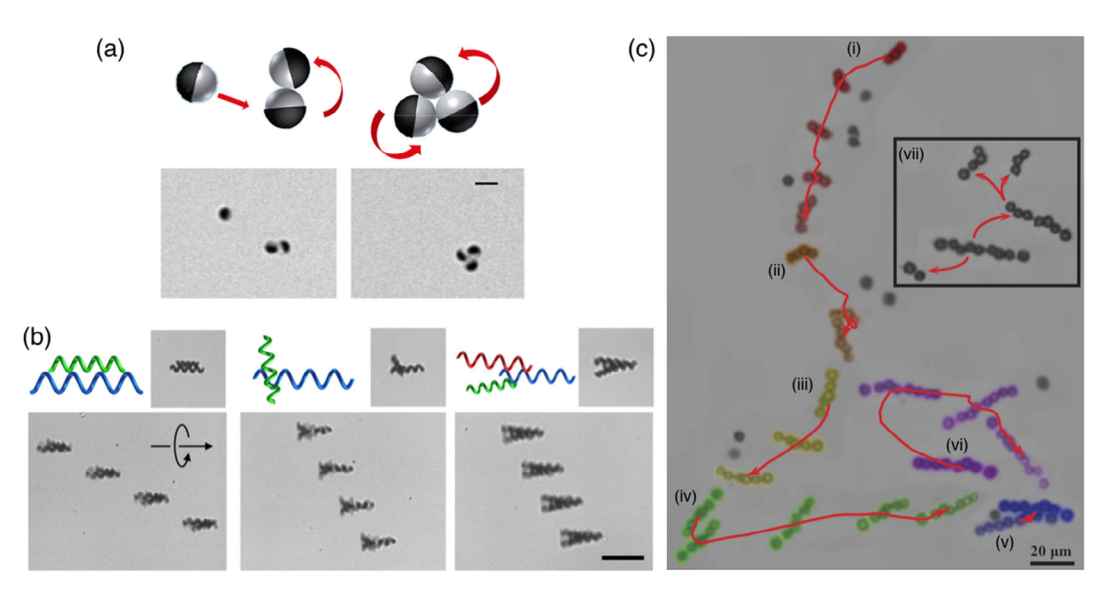


Figure 11. Dynamic assembly and disassembly of microswimmers. a) Assembly of Janus catalytic motors, where the "on-the-fly" doublet-to-triplet switching converts the circular motion of the doublet to a spinning motion of the triplet. Scale bar, 2 µm. Reproduced with permission. [172] Copyright 2013, American Chemical Society. b) Helical swimmer assemblies at different configurations captured in motion with time-lapse imaging (1.0 s apart, scale bar, 50 μm). Reproduced with permission.<sup>[173]</sup> Copyright 2013, American Chemical Society. c) Spherical particles made to assemble or disassemble on command through the manipulation of the applied external magnetic field parameters such as amplitude and frequency. Reproduced under a Creative Commons Attribution License (CC BY 4.0). [174] Copyright 2016, The Author(s). Published by Springer Nature. (i) three-bead long robotic swimmer picks up spherical magnetic beads along its journey to become four-bead long as observed at (ii), then five-bead long as observed at (iii), and continues to pick up four more spheres until it becomes nine-bead long swimmer at (vi). (vii) Nine beads break into three swimmers of 2, 3, and 4 beads, respectively.

environments and performing different tasks through dynamic reconfiguration.

Beyond simply swimming as an aggregate, another basic manipulation of a multi-microrobot system is the simultaneous control of groups of microswimmers under a single global input. Controllability of a relatively small numbers of microswimmers was demonstrated with engineered variations in geometric and magnetic properties of microswimmers, which exhibit distinct velocity responses to the same magnetic field. [177–180] The nonlinear speed-frequency relationship of magnetic swimmers above the step-out frequency can also be exploited for individual steering in multi-microrobot system. [181,182] In addition, magnetic field gradients, [183] specialized substrates, [184] and shape diversity [185] offer additional strategies to control multiple microrobots. Sorting of a large number of microswimmers based on size, [186] chirality, [187] and magnetic properties, [188] has been experimentally realized, contributing basic building blocks toward full control of microswimmers' motion. As a remark, microswimmers were also sorted with shear flows and patterned microchannels; [189,190] yet, the working conditions required for these sorting mechanisms may limit their use for in vivo medical applications.

## 5. Conclusion

The past several decades have seen tremendous progress in the development of artificial microswimmers, which led to relatively mature techniques in propelling engineered microstructures in laboratory environments. These advances lay the foundation for developing the next generation of microswimmers that can perform increasingly complicated operations in complex environments. In this Report, we have discussed recent developments in instilling intelligent behaviors into artificial microswimmers, rendering them "smart" in terms of propulsion (Section 2), navigation (Section 3), and performing complex tasks (Section 4). These intelligent behaviors are realized by integrating emerging technologies and novel approaches, including the use of soft active materials, machine learning, biohybrid, and modular microrobotics approaches, which collectively equip artificial microswimmers with different adaptive behaviors like biological cells. Although these smart microswimmers are discussed in the context of their biomedical applications, their intelligent behaviors can also be useful for other applications such as environmental monitoring and remediation.  $\hat{l}^{\hat{1}06]}$  The development of smart artificial microswimmers is only at its start and most studies surveyed in this Report are in the proof of concept stage. Subsequent developments require further integration of knowledge, approaches, and technologies across multiple disciplines. Biocompatibility and biodegradability of microswimmers become important design considerations as we get closer to their in vivo biomedical applications. [99,191] Efforts along these directions will bring us another step closer in realizing Feynman's fantasy of swallowing a "microsurgeon."

# **Acknowledgements**

O.S.P. was partially supported by NSF under grants no. EFMA-1830958 and CBET-1931292. Y.D. and E.D. are partially supported by NSAF-NSFC undergrant No. U1930402. Useful discussion with Professor Yong Lin Kong (University of Utah) is gratefully acknowledged.

www.advintellsyst.com

## Conflict of Interest

The authors declare no conflict of interest.

## **Keywords**

active particles, locomotion, microswimmers

Received: November 3, 2019 Revised: February 2, 2020 Published online: May 28, 2020

- [1] R. P. Feynman, Eng. Sci. Mag. 1960, 23. 22.
- [2] H. Berg, Random Walks in Biology, Princeton University Press, Princeton 1993.
- [3] L. J. Fauci, R. Dillon, Annu. Rev. Fluid Mech. 2006, 38, 371.
- [4] E. Lauga, Annu. Rev. Fluid Mech. 2016, 48, 105.
- [5] R. Rikmenspoel, C. A. Isles, Biophys. J. 1985, 47, 395.
- [6] Y. Magariyama, S. Y. Masuda, Y. Takano, T. Ohtani, S. Kudo, FEMS Microbiol. Lett. 2001, 205, 343.
- [7] T. J. Pedley, D. R. Brumley, R. E. Goldstein, J. Fluid. Mech. 2016, 798, 165.
- [8] R. Dreyfus, J. Baudry, M. L. Roper, M. Fermigier, H. A. Stone, J. Bibette, *Nature* 2005, 437, 862.
- [9] A. Ghosh, P. Fischer, Nano Lett. 2009, 9, 2243.
- [10] J. Simmchen, J. Katuri, W. E. Uspal, M. N. Popescu, M. Tasinkevych, S. Sánchez, Nat. Commun. 2016, 7, 10598.
- [11] H. Berg, Phys. Today 2000, 53, 24.
- [12] C. Brennen, H. Winet, Annu. Rev. Fluid Mech. 1977, 9, 339.
- [13] E. Lauga, T. R. Powers, Rep. Prog. Phys. 2009, 72, 096601.
- [14] J. M. Yeomans, D. O. Pushkin, H. Shum, Eur. Phys. J. Spec. Top. 2014, 223, 1771.
- [15] J. Elgeti, R. G. Winkler, G. Gompper, Rep. Prog. Phys. 2015, 78, 056601.
- [16] O. S. Pak, E. Lauga, Fluid-Structure Interactions in Low-Reynolds-Number Flows, Chapter 4, Royal Society of Chemistry, Cambridge, UK 2016.
- [17] D. Akin, J. Sturgis, K. Ragheb, D. Sherman, K. Burkholder, J. P. Robinson, A. K. Bhunia, S. Mohammed, R. Bashir, *Nat. Nanotechnol.* 2007, 2, 441.
- [18] O. Felfoul, M. Mohammadi, S. Taherkhani, D. de Lanauze, Y. Z. Xu, D. Loghin, S. Essa, S. Jancik, D. Houle, M. Lafleur, L. Gaboury, M. Tabrizian, N. Kaou, M. Atkin, T. Vuong, G. Batist, N. Beauchemin, D. Radzioch, S. Martel, *Nat. Nanotechnol.* 2016, 11, 941.
- [19] B. W. Park, J. Zhuang, O. Yasa, M. Sitti, ACS Nano 2017, 11, 8910.
- [20] O. Yasa, P. Erkoc, Y. Alapan, M. Sitti, Adv. Mater. 2018, 30, 1804130.
- [21] M. A. Fischbach, J. A. Bluestone, W. A. Lim, Sci. Transl. Med. 2013, 5, 179ps7.
- [22] A. S. Khalil, J. J. Collins, Nat. Rev. Genet. 2010, 11, 367.
- [23] R. W. Bradley, M. Buck, B. Wang, J. Mol. Biol. 2016, 428, 862.
- [24] M. O. Din, T. Danino, A. Prindle, M. Skalak, J. Selimkhanov, K. Allen, E. Julio, E. Atolia, L. S. Tsimring, S. N. Bhatia, J. Hasty, *Nature* 2016, 536, 81.
- [25] J. Claesen, M. A. Fischbach, ACS Synth. Biol. 2014, 4, 358.
- [26] R. W. Carlsen, M. Sitti, Small 2014, 10, 3831.
- [27] M. Sitti, H. Ceylan, W. Hu, J. Giltinan, M. Turan, S. Yim, E. Diller, Proc. IEEE 2015, 103, 205.
- [28] Z. Hosseinidoust, B. Mostaghaci, O. Yasa, B. W. Park, A. V. Singh, M. Sitti, Adv. Drug Deliv. Rev. 2016, 106, 27.

- [29] L. Ricotti, B. Trimmer, A. W. Feinberg, R. Raman, K. K. Parker, R. Bashir, M. Sitti, S. Martel, P. Dario, A. Menciassi, Sci. Robot. 2017, 2, eaaq0495.
- [30] D. T. Riglar, P. A. Silver, Nat. Rev. Microbiol. 2018, 16, 214.
- [31] J. J. Abbott, K. E. Peyer, M. C. Lagomarsino, L. Zhang, L. Dong, I. K. Kaliakatsos, B. J. Nelson, Int. J. Robot. Res. 2009, 28, 1434.
- [32] S. Ebbens, R. A. L. Jones, A. J. Ryan, R. Golestanian, J. R. Howse, *Phys. Rev. E* 2010, 82, 015304.
- [33] S. Sengupta, M. E. Ibele, A. Sen, Angew Chem., Int. Ed. 2012, 51, 8434.
- [34] C. Hu, S. Pané, B. J. Nelson, Annu. Rev. Control Robot. Auton. Syst. 2018, 1, 53
- [35] W. Gao, S. Sattayasamitsathit, K. M. Manesh, D. Weihs, J. Wang, J. Am. Chem. Soc. 2010, 132, 14403.
- [36] O. S. Pak, W. Gao, J. Wang, E. Lauga, Soft Matter 2011, 7, 8169.
- [37] L. Zhang, J. J. Abbott, L. Dong, K. E. Peyer, B. E. Kratochvil, H. Zhang, C. Bergeles, B. J. Nelson, *Nano Lett.* 2009, 9, 3663.
- [38] W. F. Paxton, S. Sundararajan, T. E. Mallouk, A. Sen, Angew. Chem., Int. Ed. 2006, 45, 5420.
- [39] J. L. Moran, J. D. Posner, Annu. Rev. Fluid Mech. 2017, 49, 511.
- [40] E. M. Purcell, Am. J. Phys. 1977, 45, 3.
- [41] X. Nassif, S. Bourdoulous, E. Eugène, P. O. Couraud, *Trends Microbiol.* 2002, 10, 227.
- [42] J. P. Celli, B. S. Turner, N. H. Afdhal, S. Keates, I. Ghiran, C. P. Kelly, R. H. Ewoldt, G. H. McKinley, P. So, S. Erramilli, R. Bansil, Proc. Natl. Acad. Sci. U. S. A. 2009, 106, 14321.
- [43] S. A. Mirbagheri, H. C. Fu, Phys. Rev. Lett. 2016, 116, 198101.
- [44] O. R. Barclay, J. Exp. Biol. 1946, 23, 177.
- [45] C. Fang-Yen, M. Wyart, J. Xie, J. Xie, R. Kawai, T. Kodger, S. Chen, Q. Wen, A. D. T. Samuel, Proc. Natl. Acad. Sci. U. S. A. 2010, 107, 20323
- [46] R. D. Maladen, Y. Ding, C. Li, D. I. Goldman, Science 2009, 325, 314.
- [47] C. Hu, S. Pané, B. J. Nelson, Annu. Rev. Contr. Robo. Auto. 2018, 1, 53.
- [48] A. M. Maier, C. Weig, P. Oswald, E. Frey, P. Fischer, T. Liedl, Nano Lett. 2016, 16, 906.
- [49] C. Ohm, M. Brehmer, R. Zentel, Adv. Mater. 2010, 22, 3366.
- [50] Y. Liu, J. K. Boyles, J. Genzer, M. D. Dickey, Soft Matter 2012, 8, 1764.
- [51] J. Mu, C. Hou, H. Wang, Y. Li, Q. Zhang, M. Zhu, Sci. Adv. 2015, 1, e1500533.
- [52] H. Zeng, P. Wasylczyk, C. Parmeggiani, D. Martella, M. Burresi, D. S. Wiersma, Adv. Mater. 2015, 27, 3883.
- [53] S. Palagi, A. G. Mark, S. Y. Reigh, K. Melde, T. Qiu, H. Zeng, C. Parmeggiani, D. Martella, A. Sanchez-Castillo, N. Kapernaum, F. Giesselmann, D. S. Wiersma, E. Lauga, P. Fischer, *Nat. Mater.* 2016, 15, 647.
- [54] R. Mohr, K. Kratz, T. Weigel, M. Lucka-Gabor, M. Moneke, A. Lendlein, Proc. Natl. Acad. Sci. U. S. A. 2006, 103, 3540.
- [55] E. Hawkes, B. An, N. M. Benbernou, H. Tanaka, S. Kim, E. D. Demaine, D. Rus, R. J. Wood, *Proc. Natl. Acad. Sci. U. S. A.* 2010, 107, 12441.
- [56] T. Xie, Nature 2010, 464, 267.
- [57] S. Felton, M. Tolley, E. Demaine, D. Rus, R. Wood, Science 2014, 345, 644.
- [58] H. W. Huang, M. S. Sakar, A. J. Petruska, S. Pané, B. J. Nelson, Nat. Commun. 2016, 7, 12263.
- [59] H. W. Huang, F. E. Uslu, P. Katsamba, E. Lauga, M. S. Sakar, B. J. Nelson, Sci. Adv. 2019, 5, eaau1532.
- [60] G. Z. Lum, Z. Ye, X. Dong, H. Marvi, O. Erin, W. Hu, M. Sitti, Proc. Natl. Acad. Sci. U. S. A. 2016, 113, E6007.
- [61] W. Hu, G. Z. Lum, M. Mastrangeli, M. Sitti, Nature 2016, 5554, 81.
- [62] V. A. Rohr, S. Trimpe, A. Marco, P. Fischer, S. Palagi, in IEEE/RSJ Int. Conf. on Intelligent Robots and Systems (IROS) 2018, 6199.
- [63] E. W. Knight-Jones, J. Cell Sci. 1954, s3-95, 503.
- [64] R. Horstmeyer, H. Ruan, C. Yang, Nat. Photonics 2015, 9, 563.

www.advancedsciencenews.com www.advintellsyst.com

[65] M. Grzybowski, M. Taki, K. Senda, Y. Sato, T. Ariyoshi, Y. Okada, R. Kawakami, T. Imamura, S. Yamaguchi, Angew. Chem., Int. Ed. 2018, 57, 10137.

- [66] N. Ji, Nat. Methods 2017, 14, 374.
- [67] S. Palagi, A. G. Mark, K. Melde, T. Qiu, H. Zeng, C. Parmeggiani, D. Martella, D. S. Wiersma, P. Fischer, in 2017 Int. Conf. on Manipulation, Automation and Robotics at Small Scales (MARSS), IEEE, Piscataway, NJ 2017, pp. 1–5.
- [68] B. Shahriari, K. Swersky, Z. Wang, R. P. Adams, N. De Freitas, *Proc. IEEE* 2015, 104, 148.
- [69] R. S. Sutton, A. G. Barto, Reinforcement Learning: An Introduction, MIT Press, Cambridge, MA 2018.
- [70] S. Colabrese, K. Gustavsson, A. Celani, L. Biferale, Phys. Rev. Lett. 2017, 118, 158004.
- [71] S. Muiños-Landin, K. Ghazi-Zahedi, F. Cichos, Reinforcement learning of artificial microswimmers. arXiv 2018: 1803.06425.
- [72] A. C. H. Tsang, P. W. Tong, S. Nallan, O. S. Pak, Self-learning how to swim at low Reynolds number. arXiv 2018: 1808.07639.
- [73] A. Najafi, R. Golestanian, Phys. Rev. E 2004, 69, 062901.
- [74] R. Dreyfus, J. Baudry, H. A. Stone, Euro. Phys. J. B 2005, 47, 161.
- [75] D. J. Earl, C. M. Pooley, J. F. Ryder, I. Bredberg, J. M. Yeomans, J. Chem. Phys. 2007, 126, 064703.
- [76] F. Alouges, A. DeSimone, L. Heltai, A. Lefebvre-Lepot, B. Merlet, Discrete Cont. Dyn.-B 2012, 18, 1189.
- [77] M. Medina-Sánchez, O. G. Schmidt, Nature 2017, 545, 406.
- [78] B. M. Friedrich, F. Jülicher, Proc. Natl. Acad. Sci. U. S. A. 2007, 104, 13256.
- [79] K. Drescher, R. E. Goldstein, I. Tuval, Proc. Natl. Acad. Sci. U. S. A. 2010, 107, 11171.
- [80] A. C. Tsang, A. T. Lam, I. H. Riedel-Kruse, Nat. Phys. 2018, 14, 1216.
- [81] V. Kantsler, J. Dunkel, M. Blayney, R. E. Goldstein, *Elife* 2014, 3, e02403.
- [82] R. Blakemore, Science 1975, 190, 377.
- [83] D. P. Häder, Arch. Microbiol. 1987, 147, 179.
- [84] S. Saha, R. Golestanian, S. Ramaswamy, Phys. Rev. E 2014, 89, 062316.
- [85] Y. Hong, N. M. K. Blackman, N. D. Kopp, A. Sen, D. Velegol, Phys. Rev. Lett. 2007, 99, 178103.
- [86] T. Bickel, G. Zecua, A. Würger, Phys. Rev. E 2014, 89, 050303.
- [87] M. Tătulea-Codrean, E. Lauga, J. Fluid Mech. 2018, 856, 921.
- [88] I. Theurkauff, C. Cottin-Bizonne, J. Palacci, C. Ybert, L. Bocquet, Phys. Rev. Lett. 2012, 108, 268303.
- [89] C. Jin, C. Krüger, C. C. Maass, Proc. Natl. Acad. Sci. U. S. A. 2017, 114, 5089.
- [90] J. Palacci, S. Sacanna, A. P. Steinberg, D. J. Pine, P. M. Chaikin, Science 2013, 339, 936.
- [91] O. Pohl, H. Stark, Phys. Rev. Lett. 2014, 112, 238303.
- [92] B. Liebchen, D. Marenduzzo, M. E. Cates, Phys. Rev. Lett. 2017, 118, 268001.
- [93] F. Ginot, I. Theurkauff, F. Detcheverry, C. Ybert, C. Cottin-Bizonne, Nat. Commun. 2018, 9, 696.
- [94] I. Lagzi, S. Soh, P. J. Wesson, K. P. Browne, B. A. Grzybowski, J. Am. Chem. Soc. 2010, 132, 1198.
- [95] J. Cejkova, M. Novak, F. Stepanek, M. M. Hanczyc, *Langmuir* 2014, 30, 11937.
- [96] W. Francis, C. Fay, L. Florea, D. Diamond, Chem. Commun. 2015, 51, 2342.
- [97] J. Shao, M. Xuan, H. Zhang, X. Lin, Z. Wu, Q. He, Angew. Chem., Int. Ed. 2017, 56, 12935.
- [98] C. Chen, X. Chang, P. Angsantikul, J. Li, B. Esteban-Fernández de Ávila, E. Karshalev, W. Liu, F. Mou, S. He, R. Castillo, Y. Liang, J. Guan, L. Zhang, J. Wang, Adv. Biosyst. 2018, 2, 1700160.
- [99] H. Wang, M. Pumera, Adv. Funct. Mater. 2018, 28, 1705421.

- [100] V. Magdanz, O. G. Schmidt, Expert Opin. Drug Delivery 2014, 11, 1125.
- [101] J. Plutnar, M. Pumera, Angew. Chem., Int. Ed. 2019, 58, 2190.
- [102] W. H. D. Jong, P. J. Borm, Int. J. Nanomed. 2008, 3, 133.
- [103] L. Abdelmohsen, F. Peng, Y. Tu, D. Wilson, J. Mater. Chem. B 2014, 2, 2395.
- [104] C. Chen, E. Karshalev, J. Guan, J. Wang, Small 2018; 14, 1704252.
- [105] A. Joseph, C. Contini, D. Cecchin, S. Nyberg, L. Ruiz-Perez, J. Gaitzsch, G. Fullstone, X. Tian, J. Azizi, J. Preston, G. Volpe, G. Battaglia, Sci. Adv. 2017, 3, e1700362.
- [106] W. Gao, J. Wang, ACS Nano 2014, 8, 3170.
- [107] D. A. Bazylinski, R. B. Frankel, Nat. Rev. Microbiol. 2004, 2, 217.
- [108] S. Klumpp, D. Faivre, Eur. Phys. J-Spec. Top. 2016, 225, 2173.
- [109] L. Zhang, J. J. Abbott, L. Dong, B. E. Kratochvil, D. Bell, B. J. Nelson, Appl. Phys. Lett. 2009, 94, 064107.
- [110] W. Gao, K. M. Manesh, J. Hua, S. Sattayasamitsathit, J. Wang, *Small* **2011**, 7, 2047.
- [111] J. Li, T. Li, T. Xu, T. Xu, M. Kiristi, W. Liu, Z. Wu, J. Wang, Nano Lett. 2015. 15. 4814.
- [112] T. R. Kline, W. F. Paxton, T. E. Mallouk, A. Sen, Angew. Chem., Int. Ed. 2005, 44, 744.
- [113] J. Burdick, R. Laocharoensuk, P. M. Wheat, J. D. Posner, J. Wang, J. Am. Chem. Soc. 2008, 130, 8164.
- [114] G. Zhao, M. Pumera, Langmuir 2013, 29, 7411.
- [115] S. Sanchez, A. A. Solovev, S. Schulze, O. G. Schmidt, Chem. Commun. 2011, 47, 698.
- [116] A. A. Solovev, S. Sanchez, M. Pumera, Y. F. Mei, O. G. Schmidt, Adv. Funct. Mater. 2010, 20, 2430.
- [117] G. Zhao, S. Sanchez, O. G. Schmidt, M. Pumera, Chem. Comm. 2012, 48, 10090.
- [118] L. Baraban, D. Makarov, R. Streubel, I. Mönch, D. Grimm, S. Sanchez, O. G. Schmidt, ACS Nano 2012, 6, 3383.
- [119] W. Zhu, J. Li, Y. J. Leong, I. Rozen, X. Qu, R. Dong, Z. Wu, W. Gao, P. H. Chung, J. Wang, S. Chen, Adv. Mater. 2015, 27, 4411.
- [120] P. S. Schattling, M. A. Ramos-Docampo, V. Salgueiriño, B. Städler, ACS Nano 2017, 11, 3973.
- [121] V. Garcia-Gradilla, J. Orozco, S. Sattayasamitsathit, F. Soto, F. Kuralay, A. Pourazary, A. Katzenberg, W. Gao, Y. Shen, J. Wang, ACS Nano 2013, 7, 9232.
- [122] S. Klumpp, C. T. LefÄšvre, M. Bennet, D. Faivre, *Phys. Rep.* **2019**; 789, 1.
- [123] B. Dai, J. Wang, Z. Xiong, X. Zhan, W. Dai, C.-C. Li, S.-P. Feng, J. Tang, Nat. Nanotechnol. 2016, 11, 1087.
- [124] J. Zheng, B. Dai, J. Wang, Z. Xiong, Y. Yang, J. Liu, X. Zhan, Z. Wan, J. Tang, Nat. Commun. 2017, 8, 1438.
- [125] C. Lozano, T. B. Hagen, H. Löwen, C. Bechinger, Nat. Commun. 2016, 7, 12828.
- [126] Z. Ye, Y. Sun, H. Zhang, B. Song, B. Dong, Nanoscale 2017, 9, 18516.
- [127] D. P. Singh, W. E. Uspal, M. N. Popescu, L. G. Wilson, P. Fischer, Adv. Funct. Mater. 2018, 28, 1706660.
- [128] Z. Zhang, J. Liu, J. Meriano, C. Ru, S. Xie, J. Luo, Y. Sun, Sci. Rep. 2016, 6, 23553.
- [129] J. Palacci, S. Sacanna, A. Abramian, J. Barral, K. Hanson, A. Y. Grosberg, D. J. Pine, P. M. Chaikin, Sci. Adv. 2015, 1, e1400214.
- [130] L. Ren, D. Zhou, Z. Mao, P. Xu, T. J. Huang, T. E. Mallouk, ACS Nano 2017, 11, 10591.
- [131] Q. Brosseau, F. B. Usabiaga, E. Lushi, Y. Wu, L. Ristroph, J. Zhang, M. Ward, M. J. Shelley, *Phys. Rev. Lett.* **2019**, *123*, 178004.
- [132] V. Kam, N. Moseyko, J. Nemson, L. J. Feldman, Int. J. Plant Sci. 1999, 160, 1093.
- [133] A. M. Roberts, J. Exp. Biol. 2010, 213, 4158.
- [134] A. M. Roberts, Biol. Bull 2006, 210, 78.
- [135] A. I. Campbell, S. J. Ebbens, Langmuir 2013, 29, 14066.

www.advintellsyst.com

- [136] T. B. Hagen, F. Kümmel, R. Wittkowski, D. Takagi, H. Löwen, C. Bechinger, Nat. Comm. 2014, 5, 4829.
- [137] B. Liebchen, P. Monderkamp, T. B. Hagen, H. Löwen, Phys. Rev. Lett. **2018**, *120*, 208002.
- [138] C. Datt, G. J. Elfring, Phys. Rev. Lett 2019, 123, 158006.
- [139] K. Takabe, H. Tahara, M. S. Islam, S. Affroze, S. Kudo, S. Nakamura, Microbiology 2017, 163, 153.
- [140] M. Y. Sherman, E. Timkina, A. Glagolev, FEMS Microbiol. Lett. 1982, 13, 137.
- [141] N. Oppenheimer, S. Navardi, H. A. Stone, Phys. Rev. Fluids 2016, 1, 014001.
- [142] P. S. Eastham, K. Shoele, Axisymmetric squirmers in stokes fluid with nonuniform viscosity. arXiv 2019: 1904.01946.
- [143] M. Laumann, W. Zimmermann, Eur. Phys. J. E 2019, 42, 108.
- [144] L. Zhang, K. E. Peyer, B. J. Nelson, Lab Chip 2010, 10, 2203.
- [145] M. S. Sakar, E. B. Steager, D. H. Kim, M. J. Kim, G. J. Pappas, V. Kumar, Appl. Phys. Lett. 2010, 96, 043705.
- [146] S. Tottori, L. Zhang, F. Qiu, K. K. Krawczyk, A. Franco-Obregón, B. J. Nelson, Adv. Mater. 2012, 24, 811.
- [147] W. Gao, D. Kagan, O. S. Pak, C. Clawson, S. Campuzano, E. Chuluun-Erdene, E. Shipton, E. E. Fullerton, L. Zhang, E. Lauga, J. Wang, Small 2012, 8, 460.
- [148] R. Mhanna, F. Qiu, L. Zhang, Y. Ding, K. Sugihara, M. Zenobi-Wong, B. J. Nelson, Small 2014, 10, 1953.
- [149] S. Sundararajan, P. E. Lammert, A. W. Zudans, V. H. Crespi, A. Sen, Nano Lett. 2008, 8, 1271.
- [150] M. Medina-Sánchez, L. Schwarz, A. K. Meyer, F. Hebenstreit, O. G. Schmidt, Nano Lett. 2015, 16, 555.
- [151] Z. Ye, E. Diller, M. Sitti, J. Appl. Phys. 2012, 112, 064912.
- [152] T. Petit, L. Zhang, K. E. Peyer, B. E. Kratochvil, B. J. Nelson, Nano Lett. 2012, 12, 156.
- [153] E. B. Steager, M. S. Sakar, C. Magee, M. Kennedy, A. Cowley, V. Kumar, Int. J. Rob. Res. 2013, 32, 346.
- [154] H. W. Tung, K. E. Peyer, D. F. Sargent, B. J. Nelson, Appl. Phys. Lett. **2013**, *103*, 114101.
- [155] Y. Zhou, M. Sitti, Lab Chip 2014, 14, 2177.
- [156] T. Y. Huang, F. Qiu, H. W. Tung, X. B. Chen, B. J. Nelson, M. S. Sakar, Appl. Phys. Lett. 2014, 105, 114102.
- [157] G. Mishler, A. C. H. Tsang, O. S. Pak, J. Nonlinear Sci. 2018, 28, 1379.
- [158] F. Martínez-Pedrero, P. Tierno, J. Colloid Interf. Sci. 2018, 519, 296.
- [159] S. Lee, S. Kim, S. Kim, J.-Y. Kim, C. Moon, B. J. Nelson, H. Choi, Adv. Healthc. Mater. 2018, 7, 1700985.
- [160] T. Y. Huang, M. S. Sakar, A. Mao, A. J. Petruska, F. Qiu, X.-B. Chen, S. Kennedy, D. Mooney, B. J. Nelson, Adv. Mater. 2015, 27, 6644.
- [161] U. Bozuyuk, O. Yasa, I. C. Yasa, H. Ceylan, S. Kizilel, M. Sitti, ACS Nano 2018, 12, 9617.
- [162] S. Sundararajan, S. Sengupta, M. E. Ibele, A. Sen, Small 2010, 6, 1479.

- [163] H. Ceylan, I. C. Yasa, O. Yasa, A. F. Tabak, J. Giltinan, M. Sitti, bioRxiv 2018, 379024.
- [164] A. Servant, F. Qiu, M. Mazza, K. Kostarelos, B. J. Nelson, Adv. Mater. 2015. 27. 2981.
- [165] A. A. Solovev, S. Sanchez, O. G. Schmidt, Nanoscale 2013, 5, 1284.
- [166] D. Saintillan, Annu. Rev. Fluid Mech. 2018, 50, 563.
- [167] R. W. Carlsen, M. R. Edwards, J. Zhuang, C. Pacoret, M. Sitti, Lab Chip 2014, 14, 3850.
- [168] D. D. Lanauze, O. Felfoul, J. P. Turcot, M. Mohammadi, S. Martel, Int. I. Rob. Res. 2014, 33, 359.
- [169] D. Loghin, C. Tremblay, M. Mohammadi, S. Martel, Int. J. Rob. Res. **2017**, 36, 1195.
- [170] K. Bente, A. Codutti, F. Bachmann, D. Faivre, Small 2018, 14, 1704374.
- [171] S. Ni, E. Marini, I. Buttinoni, H. Wolf, L. Isa, Soft Matter 2017, 13, 4252.
- [172] W. Gao, A. Pei, X. Feng, C. Hennessy, J. Wang, J. Am. Chem. Soc. 2013, 135, 998.
- [173] S. Tottori, L. Zhang, K. E. Peyer, B. J. Nelson, Nano Lett. 2013, 13, 4263.
- [174] U. K. Cheang, F. Meshkati, H. Kim, K. Lee, H. C. Fu, M. J. Kim, Sci. Rep. 2016, 6, 30472.
- [175] P. J. Vach, D. Faivre, Sci. Rep. 2015, 5, 9364.
- [176] R. Niu, T. Palberg, Soft Matter 2018, 14, 7554.
- [177] K. Ishiyama, M. Sendoh, K. Arai, J. Magn. Magn. Mater. 2002, 242-245, 41.
- [178] S. Tottori, N. Sugita, R. Kometani, S. Ishihara, M. Mitsuishi, J. Micro-Nano. Mechatron. 2011, 6, 89.
- [179] E. Diller, S. Floyd, C. Pawashe, M. Sitti, IEEE Trans. Rob. 2012, 28, 172.
- [180] U. Kei Cheang, K. Lee, A. A. Julius, M. J. Kim, Appl. Phys. Lett. 2014, 105, 083705.
- [181] A. W. Mahoney, N. D. Nelson, K. E. Peyer, B. J. Nelson, J. J. Abbott, Appl. Phys. Lett. 2014, 104, 144101.
- [182] P. J. Vach, S. Klumpp, D. Faivre, J. Phys. D: Appl. Phys. 2015, 49, 065003.
- [183] E. Diller, J. Giltinan, M. Sitti, Int. J. Rob. Res. 2013, 32, 614.
- [184] D. Cappelleri, D. Efthymiou, A. Goswami, N. Vitoroulis, M. Zavlanos, Int. J. Adv. Rob. Syst. 2014, 11, 150.
- [185] F. Bachmann, K. Bente, A. Codutti, D. Faivre, Phys. Rev. Applied 2019, 11, 034039.
- [186] P. J. Vach, N. Brun, M. Bennet, L. Bertinetti, M. Widdrat, J. Baumgartner, S. Klumpp, P. Fratzl, D. Faivre, Nano Lett. 2013, 13, 5373.
- [187] D. Schamel, M. Pfeifer, J. G. Gibbs, B. Miksch, A. G. Mark, P. Fischer, J. Am. Chem. Soc. 2013, 135, 12353.
- [188] T. A. Howell, B. Osting, J. J. Abbott, Phys. Rev. Appl. 2018, 9, 054021.
- [189] F. H. C. Marcos, T. R. Powers, R. Stocker, Phys. Rev. Lett. 2009, 102, 158103.
- [190] M. Mijalkov, G. Volpe, Soft Matter 2013, 9, 6376.
- [191] E.-F. B. Avila, P. Angsantikul, J. Li, W. Gao, L. Zhang, J. Wang, Adv. Funct. Mater. 2018, 28, 1705640.